# CHARACTERIZATION OF FLEXIBLE ANTENNAS FOR WIRELESSLY POWERING MEDICAL IMPLANTS

by

SAFWAN AHMED MUNEER

Presented to the Faculty of the Graduate School of
The University of Texas at Arlington in Partial Fulfillment
of the Requirements
for the Degree of

MASTER OF SCIENCE IN ELECTRICAL ENGINEERING

THE UNIVERSITY OF TEXAS AT ARLINGTON

August 2012

ACKNOWLEDGEMENTS

It is with great pleasure that I am writing this thesis work, because it marks the end of my curriculum requirements for getting my Master's degree in Electrical Engineering. I am grateful to Allah for his blessings and my family for their infinite support in pursuing my dream. Especially the sacrifice made by my mother cannot be forgotten. I am thankful to my late father whose dream was to get his children the highest quality of education; sadly he is not there to see his dream achieve fruition.

Without the help and support of Dr. JC Chiao, this work would have been incomplete. I am grateful to him for financially supporting me and for assisting me in every part of my thesis work. Dr. Hung Cao played an instrumental role in my thesis work; I would like to take this opportunity in thanking him. I am grateful to Dr. Sanchali Deb, Uday Shankar Tata, and Mathew Lee Oseng for helping me be a better individual and for giving me suggestions time and again. I would like to thank Dr. Mingyu Lu for providing me the technical platform I needed to start my thesis work. Lastly I would like to thank iMems group whose help and support made my life easy.

I would like to end my thank you list by extending a special thanks to my thesis committee members – Dr. W. Alan Davis and Dr. William E. Dillon for reading my thesis and being in the defense committee.

July 12, 2012

ABSTRACT

CHARACTERIZATION OF FLEXIBLE ANTENNAS

FOR WIRELESSLY POWERING

MEDICAL IMPLANTS

Safwan Ahmed Muneer, M.S.

The University of Texas at Arlington, 2012

Supervising Professor: JC Chiao

To minimize the trouble experienced by the patient in undergoing invasive surgeries to replace non rechargeable batteries that are used to power body implants inside, medical experts and engineers are emphasizing on making use of wireless power. Since body implant powering from external wireless power requires a source that can be easily worn outside the body, a special type of integrated antenna was implemented on a flexible substrate that conforms to the shape of the stomach curvature, thus adding increased patient comfort. The antenna bend is concave which adds to increased focus and power transfer efficiency to power the body implant. Since the dielectric constant of body cells increases with the increase in the frequency of operation of the system, the frequency used is 1.3 MHz which is in the ISM band. Since research is underway to develop a whole new kind of body implants such as retinal implants, intracranial brain computer interfaces (BCI) etc., the demand for efficient powering of

body implants from the outside using a compact source has increased to a great extent. In this research work, a square planar spiral antenna was fabricated using copper tape and mask on a flexible substrate – kapton (polyimide) to power the tag antenna (body implant). A Class – E power amplifier was used to amplify the signal before transmitting it through the reader antenna to the tag antenna which in practical implementation would be attached to the body implant. A non - planar antenna made using 24 AWG magnet wire on a Styrofoam substrate was used to receive the power. Both the reader antenna and tag antenna were resonated using appropriate capacitors to achieve maximum power transfer. In order to understand the power transfer pattern in a human body through the stomach, a stable setup and curvatures of different size were used. Since the reader antenna will be worn in the form of a belt, it was bent at different radii of curvature. The tag antenna or the reader antenna can move sideways or radially, experiments were executed to incorporate all these effects and the results for the power transfer efficiency were recorded. Accidently, it was found that the power transfer efficiency increased when the reader antenna was bent rather than straight. The feasibility of the efficiency pattern that is obtained by displacing the reader and tag antennas is confirmed by fabricating antennas with different designs and obtaining the repeatable pattern. This pattern can be used as a reference pattern to optimize the parameters of the reader antenna for optimum power transfer efficiency. Ansoft HFSS, simulation software that makes use of finite element method (FEM) to perform 3D electromagnetic simulations was used to simulate the inductance of the reader antenna. The reader antenna 3D model made using the software was bent to emulate the reader antenna bend along the stomach curvature, using AutoCAD software and Bonzai 3d software and the model was imported into HFSS and the simulations were verified with the experiment. HFSS simulations were also verified using equations given by T.H Lee in [17]. Thus, the experimental results, simulation results, and results obtained from equations were in good agreement with each other. The simulation work was thus used as a proof of concept for antenna design.

TABLE OF CONTENTS

LIST OF ILLUSTRATIONS

Figure Page

LIST OF TABLES

# CHAPTER 1

## INTRODUCTION

Healthcare to anyone, anytime and anywhere by removing locational, time and other restraints is the vision of “Pervasive Healthcare” [1]. The introduction of wireless technologies in healthcare environment has led to an increased accessibility to healthcare providers, more efficient tasks and processes, and a higher overall quality of healthcare services. Health monitoring can be used to monitor physical health, emotional health, and behavioral health. Health monitoring involves measuring several medical parameters simultaneously over a long term without interrupting the patient in performing his daily chores. Measurements can include recording and digitization of vital signs like acid, non – acid reflux in the esophagus, blood pressure, electrocardiogram (ECG), respiration rate, pulse, oxygen saturation, gastro paresis etc. The monitoring system should transmit both routine vital signs and alerting signals, when the obtained vital signs cross a particular threshold value. Comprehensive health monitoring systems include monitoring using network systems such as those networks which are implemented by using Adhoc wireless technology, personal area networks implemented by Zigbee Technology, RFID technology, large area networks implemented by Wi-Fi Technology, cellular networks etc. With the coverage and scalability provided by wireless networks used in wireless health monitoring systems, a large coverage which includes coverage through rural and urban areas covering both indoor and outdoor environments can be provided. A new feature has been added to the ongoing revolution in wireless health monitoring technologies and the term coined for this new feature is – mHealth.

mHealth or mobile health is a term used for usage of mobile communication devices such as mobile phones, tablet computers, PDA for providing health services and information.

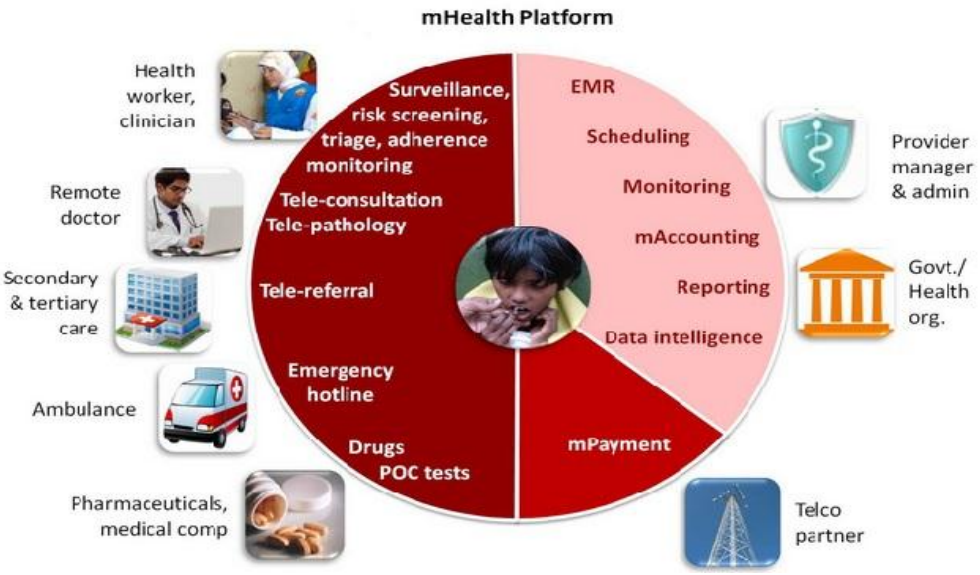


Figure 1.1 mHealth platform [31]

On the contrary, many challenges are being faced in providing better health services, such as a significant number of medical errors, considerable stress on health care providers, an increased cost of healthcare services and an exponential increase in the number of seniors and retirees in developing countries. Worldwide, there has been an increase in the number of people suffering from physical and cognitive diseases, and with the aging of world population, this number will grow even more significantly in the future. About 37 million people (which is about 14% of the world population) in the United States alone are suffering from some or the other form of disability. About 40% of seniors in the United States are suffering from disabilities. It has been shown that health monitoring can reduce the number of readmissions for patients suffering from chronic health problems. To support the long – term health care needs of the patients, comprehensive wireless health care monitoring solutions must be developed for homes, nursing homes and hospitals. As a result of the comprehensiveness of such systems, many challenges need to be taken care of in designing and developing such systems, including diverse

requirements of health monitoring, wireless and efficient powering of the body implants that are used to monitor the patients, medical decision making on the health care needs of the patients, patient comfort in wearing the powering device to power the body implant. In this thesis work problems related to wireless efficient powering of body implant and patient comfort in wearing the powering device – planar spiral antenna along with transmitter circuit are addressed by characterizing a flexible antenna.

## 1.1 Importance of wireless power

Electronic devices can be worn around the body or implanted inside the body and they can be used to perform a variety of prosthetic, therapeutic and diagnostic functions [2]. However efficiently powering the body implants is a problem, and researchers are laying a lot of emphasis on studying and solving these problems. For a long time medical practitioners have implanted body electronics inside the body which were powered by non – rechargeable batteries. This involved repetitive surgeries to replace the batteries. In order to solve this problem, wireless power transfer technology was used. There are several ways to transfer wireless power to power the body implants - magnetic resonance coupling and capacitive coupling.

In this thesis work, the body implant is powered using resonant magnetic coupling phenomenon. An advantage of making use of the coupling phenomenon is that more than one body implant can be powered using a single source.

## 1.2 Antenna characterization

The effectiveness with which body implants can be powered can be learned by studying the radiation pattern of the device that is used to power the implant. In order to study the radiation pattern of a device, one of the methods adopted is studying the efficiency pattern. The efficiency pattern of the radiating device is studied by making use of a stable setup, so that experiments performed are repeatable. Also the stability of the setup matters when the power transferred is low in order to minimize voltage fluctuations at the receiver end. In this thesis

work, the setup was made by using thick acrylic boards and pvc pipes to ensure that antenna bend is perfect, and results obtained are accurate.

### 1.2.1 Antenna efficiency

The definition of antenna efficiency inside a lossy media is not obvious, since the far – field is attenuated [6]. The standard definition of antenna gain is G(θ,φ) = ηD(θ,φ) where η is the efficiency factor, D(θ,φ) is the directivity of the antenna and is defined from the normalized power pattern $P_n$ as

$$D(\theta,\phi) = \frac{P_n(\theta,\phi)}{P_n(\theta,\phi)_{average}} = \frac{\left|\vec{F}(\theta,\varphi)\right|^2}{\left|\vec{F}(\theta,\phi)\right|^2_{average}} \tag{1.1}$$

where $\vec{F}(\theta,\phi)$ is the far-field amplitude. The normalized power pattern $P_n$ as defined from the Poynting vector, S = $\vec{S}.\hat{r}$ , is

$$P_n(\theta,\phi) = \frac{S(\theta,\phi)}{S(\theta,\phi)_{\max}} = \frac{\left|\vec{F}(\theta,\phi)\right|^2}{\left|\vec{F}(\theta,\phi)\right|^2_{\max}} \tag{1.2}$$

where the far-field amplitude is defined as

$$\vec{F}(\theta,\phi) = \lim_{|k|r\to\infty} \vec{E}(r,\theta,\phi)kre^{jkr} \tag{1.3}$$

The far-field amplitude can also be expressed as

$$\vec{F}(\theta,\phi) = -j\omega\mu k(\vec{I} - \hat{r}\hat{r}).\int_{V_s} e^{jk\vec{r}}\vec{J_s}(\vec{r})dv' \tag{1.4}$$

where $\vec{J_s}(\vec{r'})$ is the source current density in a volume $V_s$.

This definition also applies to antennas inside lossy media. The radiating power of an antenna gets attenuated by matter as it travels inside a lossy medium. This has the consequence that the position of the origin is important as it influences the shape of the pattern.

This is the reason why Antenna characterization experiments in this thesis have been performed by using different orientations of the origins of both the antennas.

The definition of antenna efficiency inside a lossy medium has to be adopted rather than the one used in air. The usual way of defining antenna efficiency is

$$\eta_{lossless} = \frac{P_{radiated}}{P_{accepted}} \tag{1.5}$$

Here $P_{accepted}$ is the power that is accepted by the transmitting antenna, i.e., the input power to the antenna subtracted from the reflected power from the transmitting antenna. In the case of an antenna in matter this definition has to be modified, as the quantity $P_{radiated}$ will vary with the radius r. The radiated power is dependent on distance between the transmitting and receiving antenna.

$P(r) = P_o e^{-2Im[k]r}$ where r is the radius at which the power is calculated and k is the dispersion constant. Antenna efficiency in a lossy matter is defined as

$$\eta_{lossy} = \frac{P_o}{P_{accepted}} \tag{1.6}$$

where $P_O$ is the radiated power. The above definition is also valid for a lossless medium.

## 1.3 Contemporary antennas used for medical implants

The antennas used for powering medical implants are – dipole antenna, wire Antenna, circumferential quarter wave, circumferential PIFA (planar inverted F antennas), patch and magnetic coil antennas.

Wire antennas such as dipole antennas [4] cannot be used at operating frequencies of 1.3 MHz, because for them to operate efficiently and resonate at the frequency of interest, they have to be half wavelength long. This is around 233 meters. Antennas of such size cannot be used to power medical implants and hence are not feasible.

Circumferential quarter wave antennas are compact plates of circular shape. They have high bandwidths, but their physical size is frequency dependent.

Circumferential PIFA and patch antennas are frequency dependent antennas. Their physical size will change with change in frequency of interest. Moreover more time and effort is needed to fabricate these antennas, and it is difficult to make them work properly at wide bandwidths. Also the physical size of these antennas will be very large if they are designed for 1.3 MHz, which is the frequency of interest in this thesis.

Magnetic coil antennas have the advantage that the resonant radiation frequency can be controlled by using a resonant circuit instead of the physical size of the structure. One such example of magnetic coil antennas is a spiral antenna.

## 1.4 Present work

In the present work, a special type of spiral antenna called flexible spiral antenna has been used. There are many advantages of making use of flexible spiral antennas –

- They are flexible; so they can bend to the shape of an object on which they are placed. In the present work they are placed on the stomach, where they take the shape of the stomach.
- Spiral antenna coil turns are distributed across the radii [3], rather than concentrated on the outer radius of the antenna. Zeirhofer and Hochmair (1996) studied the enhancement of magnetic coupling between coils and found that the magnetic coupling increases when the turns are distributes across the radii.
- Spiral antennas are frequency independent. The physical antenna size need not have to be altered if the frequency of interest changes. Changes have to only be made on the resonating circuit to achieve high efficiency at the frequency of interest.
- Spiral antennas used are planar and compact, and they can be mounted easily on the surface of interest. They do not obstruct movement of the user and are called low profile antennas.
- They are economically cheap to fabricate and the failure rate of the fabrication process is less than that of patch antennas. Also fabrication time is short.

- The polarization, radiation pattern, and impedance of such antennas remain unchanged for large bandwidths.
- When the antenna shape is made to conform to the shape of the human stomach, the antenna bends in a concave manner, this results in increase in efficiency, since all the magnetic field is focused on the medical implant.
- The bandwidth of operation of such antennas can be as high as 30:1; hence they can be used for wideband applications.
- Although the inductors used in the design have small Q values, their inductances are defined over a broad range of process variations.

The spiral antennas that were fabricated in this work are square in shape, because it is easier to fabricate antennas of this shape using the copper tape method instead of circular or trapezoidal shaped antennas. Also these antennas can be easily modeled using the three dimensional electromagnetic finite element based software called Ansoft HFSS. Using this software the antenna inductance can be verified with experiments and equations written by T.H Lee in [17].

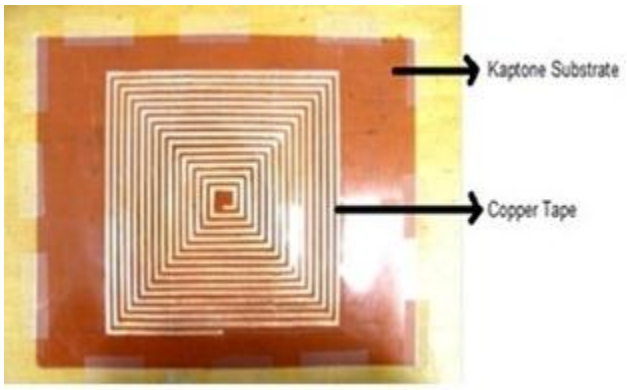


Figure 1.2 Fabricated planar spiral antenna

## 1.5 Thesis indexing

Chapter 1 deals with the issues faced in health monitoring, importance of wirelessly powering medical implants, the different types of antennas used in wireless powering of implants and the advantages of making use of flexible planar spiral antennas.

Chapter 2 deals with an introduction to spiral antennas, the different types of spiral antennas used and the design formulas associated with planar spiral antennas. It describes the different fabrication techniques used and the steps involved in fabrication, advantages and disadvantages of techniques used.

Chapter 3 gives an introduction to finite element method (FEM) simulations, used by the 3D electromagnetic simulation software – Ansoft HFSS. It describes the method involved in setting up the simulation parameters and simulation model. It describes the different steps used to verify the simulations i.e. using theoretical equations, publication results, flat antenna and bend antenna experimental results.

Chapter 4 gives an introduction to the Class – E power amplifier circuit. It describes the typical parameters that are to be considered for carrying out antenna characterization experiments, an introduction to the design and fabrication of the stable setup, an introduction to the experimental parameters, graphical results obtained by carrying out different types of experiments for antenna characterization, and the explanation of the results obtained.

Chapter 5 gives the conclusion of the Antenna characterization experiments.

Chapter 6 describes the method used to carry out future antenna characterization experiments. It also describes the method used to increase the range of power transfer.

# CHAPTER 2

# PLANAR SPIRAL ANTENNAS

## 2.1 Introduction

The numerous applications of electromagnetics to the advances of technology have necessitated the exploration and utilization of most of the electromagnetic spectrum [22]. In addition, the advent of broadband systems, have demanded the design of broadband radiators. The use of simple, small, lightweight, and economical antennas designed to operate over the entire frequency band of a system, would be most desirable. Although in practice all the desired features and benefits cannot easily be derived from a single radiator, most can effectively be accommodated. Previous to the 1950's, antennas with broadband pattern and impedance characteristics had bandwidths not greater than 2:1. In the 1950's, a breakthrough in the antenna revolution was made which extended the bandwidth to as great as 40:1 or more. The antennas introduced by the breakthrough were referred to as frequency independent, and they had geometries that were specified by angles between spiral arms. One such example of frequency independent antennas is planar spiral antennas.

Planar spiral antennas are viable candidates for near field wireless power transmission to the next generation of high performance medical implants with extreme size constraints. So far, antenna coils for powering medical implants have been fabricated with thin wires using sophisticated winding machinery [16]. However, the need for much smaller footprints in the next generation of high performance implantable devices calls for higher geometrical precision and potential for integration on chip or on package. This would require different fabrication techniques that would result in well-defined planar structures. Also these antennas offer more flexibility in defining their characteristics. A simple change in their shape could change the

polarization pattern. Planar antennas of different shapes are being studied to investigate which shapes are best for powering medical implants.

## 2.2 Different types of spiral antennas

There are different types of spiral antennas such as equiangular spiral antennas or log periodic spiral antennas, archimedean spiral antennas and cavity backed slot antennas [21]. These will be discussed in the following sections.

### 2.2.1 Equiangular spiral antenna

The log - periodic spiral antenna or the equiangular spiral antenna has each arm defined by the polar function $r = R_o e^{a\Phi}$ where $R_o$ is a constant that controls the initial radius *r* of the spiral antenna. The parameter *a* controls the rate at which the spiral antenna flares or grows as it turns. The above equation states that the spiral antenna radius grows exponentially as it turns. A plot of log – periodic spiral antenna is shown below

Figure 2.1 Equiangular spiral antenna [31]

The planar spiral antenna of Figure 2.1 will have peak radiation directions into and out of the screen (broadside to the plane of the spiral, in both the front and the back). The antenna will radiate right hand circularly polarized fields out of the screen, and left hand circularly polarized fields into the screen. The parameters that affect the radiation of the spiral antenna include:

1. The outer radius ($R_{spiral}$) – This parameter determines the lowest frequency of operation of the spiral antenna.

$$f_{low} = \frac{c}{\lambda_{low}} = \frac{c}{2\pi R_{spiral}} \quad (2.1)$$

2. The flare rate (a) – The rate at which the spiral grows with angle is the flare rate. If it is too small, the spiral is tightly wrapped around itself.
3. Feed structure – The feed must be controlled with a balun so that the spiral has balanced currents on either arm. Also, the highest frequency in the spiral antenna's operating band depends on the innermost radius of the spiral $R_o$.

$$f_{Upper} = \frac{c}{\lambda_{Upper}} = \frac{c}{4R_o} \quad (2.2)$$

4. Number of turns (N) – This is also a design parameter for the spiral antenna.

Radiation occurs from the spiral antenna when the current in the spiral arms are in phase.

### 2.2.2 Archimedean spiral antenna

Each arm of the Archimedean spiral is defined by the equation $r = a\phi$. This equation states that the radius r of the antenna increases linearly with the angle $\phi$. The parameter a, is simply a constant that controls the rate at which the spiral flares out. The second arm of the archimedean spiral is the same as the first, but rotated 180 degrees. A plot of the Archimedean spiral is shown below

Figure 2.2 Archimedean spiral antenna [31]

### 2.2.3 Cavity-backed slot antenna

The antennas discussed till now are those that are planar slot antennas. They can be used in metallic backed objects such as aircraft body etc. It is desirable for the slot antenna to be cavity backed, because this isolates the antenna from what is behind it, so that it can be mounted on objects without worrying about retuning the antenna. These antennas come in two types.

The first is a simple metallic backing separated from the antenna by some distance d. This metallic backing will cause reflections of the radiated fields that enter the cavity, and these often cancel the radiated fields that travel broadside to the plane of the antenna. If the depth *d* is an integer multiple of half wavelength, the reflected field will tend to cancel the forward travelling field of the spiral antenna, thus leading to poor radiation. Hence the wideband characteristics of a metallic cavity backed slot antenna are less. An alternate method is to make use of absorbing material to cavity back the spiral antenna. In this case, the reflected fields from the cavity will be attenuated, so that there is no destructive interference, so the antenna will maintain its wideband characteristics. This however tends to decrease the efficiency of the spiral antenna, since roughly half the radiated power is radiated. However, this loss of efficiency is 3 dB, which is often tolerable. An example of the cavity backed slot antenna is the cavity backed Archimedean spiral antenna is shown below.

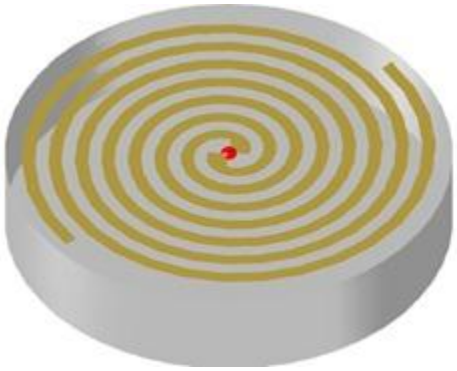

Figure 2.3 Cavity backed slot antenna [31]

## 2.3 Formulas used for planar spiral antennas

There are some formulas that accurately express the dc inductance of square, hexagonal, octagonal, and circular spiral inductors [17]. The accuracy of these expressions was modeled using field solver simulations, ASITIC, and using measurement data. For a given shape, an inductor is completely specified by the number of turns, n, the turn width w, the turn spacing s, the outer diameter $d_{out}$, the inner diameter $d_{in}$, the average diameter $d_{avg} = 0.5(d_{out} + d_{in})$ and the fill ratio defined as $\rho = \frac{(d_{out} - d_{in})}{(d_{out} + d_{in})}$. The thickness of the inductor has a meager effect on the inductance and hence is ignored. The expressions for inductance are defined in [17].

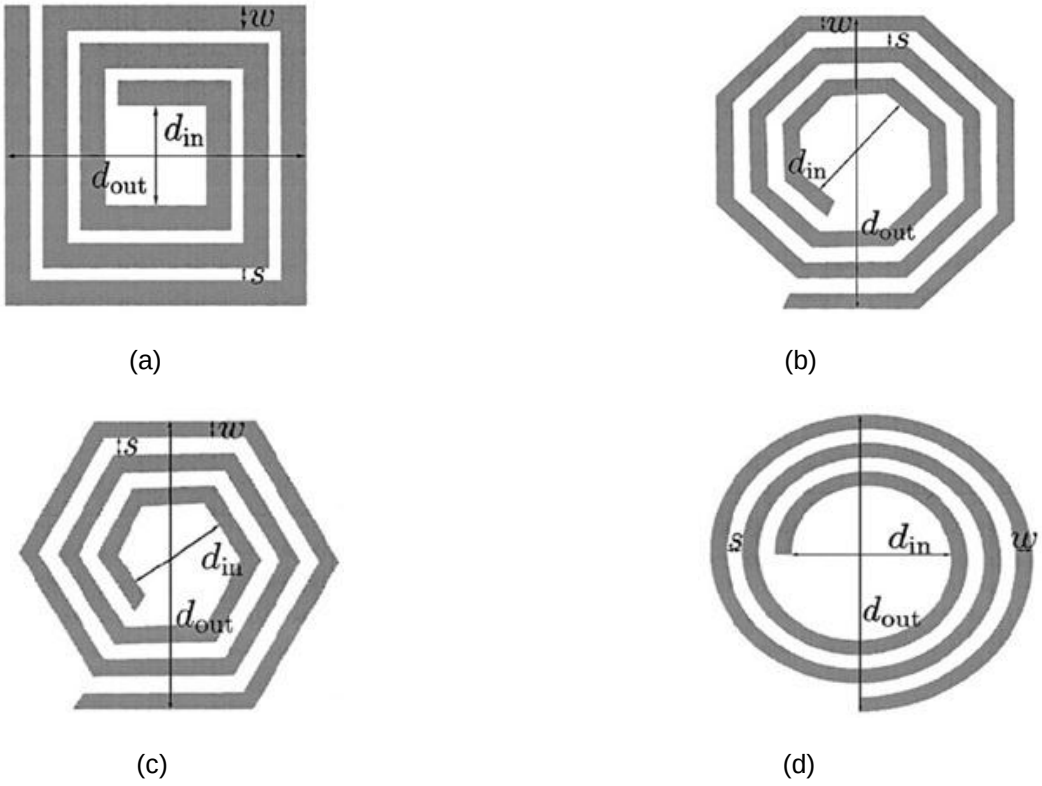


Figure 2.4 (a) Square, (b) Octagonal, (c) Hexagonal and (d) Circular planar spiral antennas [17]

### 2.3.1 Modified wheeler formula

Wheeler presented several formulas for planar spiral inductors, which were intended for discrete inductors. A simple modification of the wheeler formula can be used to obtain an expression that is valid for planar spiral integrated inductors.

$$L_{mw} = K_1 \mu_o \frac{n^2 d_{avg}}{1 + k_2 \rho} \tag{2.3}$$

where $\rho$ is the fill ratio defined, previously. The coefficients $K_1$ and $K_2$ are layout dependent and are shown in Table 2.1. The ratio, $\rho$ , is the fill ratio and represents how hollow the inductor is. For a smaller ratio the inductor is hollow, and for a larger ratio the inductor is full. Two inductors with the same average diameter but with different fill ratios will have different inductances. The full inductor has a smaller inductance because its inner turns are closer to the center of the spiral and hence would contribute less positive mutual inductance and more negative mutual inductance

| Layout | K1 | K2 |
|---|---|---|
| Square | 2.34 | 2.75 |
| Hexagonal | 2.33 | 3.82 |
| Octagonal | 2.25 | 3.55 |

Table 2.1 Modified wheeler formula constants

### 2.3.2 Expression based on current sheet approximation

Another simple and accurate expression for planar spiral inductances can be obtained by approximating the sides of the spirals by symmetrical current sheets of equivalent current densities. For example, in case of a square, 4 identical current sheets are obtained. The current sheets on opposite sides are parallel to each other, whereas the adjacent ones are orthogonal to each other. Using symmetry and the fact that orthogonal current sheets have zero mutual inductance, the computation of the inductance is now reduced to evaluating the self-inductance of one sheet and the mutual inductance between the opposite current sheets. The self and

mutual inductances are evaluated using the concepts of geometric mean distance, arithmetic mean distance, and the arithmetic mean square distance. The resulting expression [17] is

$$L_{gmd} = \frac{\mu n^2 d_{avg} c_1}{2}\left(\ln\left(\frac{c_2}{\rho}\right) + c_3\rho + c_4\rho^2\right) \tag{2.4}$$

where $c_i$ are layout dependent given by the values in Table 2.2, s and w are the spacing between the inductor turns and width of the inductor turns. Although the accuracy of the expression reduces as the ratio, s/w, becomes large, it exhibits a maximum error of 8 % for s ≤ 3w.

| Layout | c1 | c2 | c3 | c4 |
|---|---|---|---|---|
| Square | 1.27 | 2.07 | 0.18 | 0.13 |
| Hexagonal | 1.09 | 2.23 | 0 | 0.17 |
| Octagonal | 1.07 | 2.29 | 0 | 0.19 |
| Circle | 1 | 2.46 | 0 | 0.2 |

Table 2.2 Current sheet approximation formula constants

### 2.3.3 Data fitted monomial expression

This expression for inductance is obtained using a data fitting technique. The expression is given by (2.5).

$$L_{mon} = \beta d_{out}^{\alpha_1} \omega^{\alpha_2} d_{avg}^{\alpha_3} n^{\alpha_4} s^{\alpha_5} \tag{2.5}$$

where the coefficients β and $\alpha_i$ are layout dependent and given in Table 2.3. The above expression is monomial in the variables $d_{out}, \omega, d_{avg}, n$ and s. The coefficients in (2.5) were obtained using the following expressions $x_1 = \log d_{out}$, $x_2 = \log \omega$, $x_3 = \log d_{avg}$, $x_4 = \log n$, $x_5 = \log s$. Using logarithms, the expression (2.5) can be expressed as (2.6).

$$y = \log L = \alpha_o + \alpha_1 x_1 + \alpha_2 x_2 + \alpha_3 x_3 + \alpha_4 x_4 + \alpha_5 x_5 \tag{2.6}$$

where $\alpha_o = \log \beta$. This is a linear plus constant model of y as a function of x, and is easily fit by various data fitting and regression techniques. To develop the models, a simple least squares fit is used. Also $\alpha_i$ is chosen to minimize (2.7).

$$\sum_{k=1}^{N} (y^{(k)} - \alpha_o - \alpha_1 x_1^{(k)} - \alpha_2 x_2^{(k)} - \alpha_3 x_3^{(k)} - \alpha_4 x_4^{(k)} - \alpha_5 x_5^{(k)})^2 \qquad (2.7)$$

where the sum is over a family of 19000 inductors.

| Layout | β | $\alpha_1$ ($d_{out}$) | $\alpha_2$(w) | $\alpha_3$($d_{avg}$) | $\alpha_4$(n) | $\alpha_5$(s) |
|---|---|---|---|---|---|---|
| Square | $1.62*10^{-3}$ | -1.21 | -0.147 | 2.4 | 1.78 | -0.03 |
| Hexagonal | $1.28*10^{-3}$ | -1.24 | -0.174 | 2.47 | 1.77 | -0.049 |
| Octagonal | $1.33*10^{-3}$ | -1.21 | -0.163 | 2.43 | 1.75 | -0.049 |

Table 2.3 Data fitted monomial expression constants

The monomial expression (2.5) is useful since, like the other expressions (2.3), (2.4), it is accurate and simple. It is used in optimal design of inductors

## 2.4 Planar spiral antenna fabrication techniques

There are different methods adopted in this research to fabricate the planar spiral antennas. However, after making use of many methods, copper tape method was found to be the easiest. The methods used are listed below.

### 2.4.1 Photolithography process

The steps used in fabricating the planar antenna using the photolithography process are as follows

a. The edges of a desensitized double sided copper clad board are smoothened using an electric razor blade.
b. The mask is prepared using the AutoCAD program and printed on the rough side of a plastic transparency. This is placed on the photoresist coated copper clad board.

c. A sheet of Plexiglas is placed on the mask and the board, ultra violet light is used to expose the sensitized board with the mask for 10-15 minutes.

d. The exposed part of the photoresist is then washed away using potassium hydroxide solution in a beaker.

e. A 1:1 mixture of 30% hydrogen peroxide solution and hydrochloric acid is used to etch the copper from the board.

f. Acetone is then used to remove the unexposed photoresist. The planar spiral antenna is then ready to be used.

Figure 2.5 Mask for photolithography process

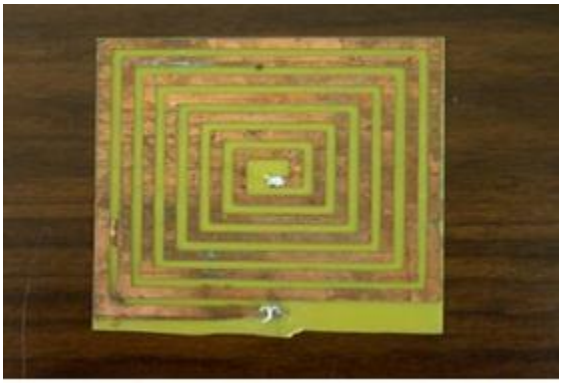

Figure 2.6 Fabricated antenna using photolithography process

2.4.1.1 Advantages of photolithography process

The process is less time consuming. It takes about half an hour to complete the antenna fabrication process. The precision achieved is high as compared to other fabrication techniques

2.4.1.2 Disadvantages of photolithography process

The process is relatively expensive, because we are making use of different chemicals, FR4 substrate. The process is very smelly, because of the release of hydrochloric acid vapors during the etching process, which are corrosive in nature.

Since FR4 substrate can be used only once for antenna fabrication, different antenna designs can only be executed using different substrates. This technique was discarded for cost reasons.

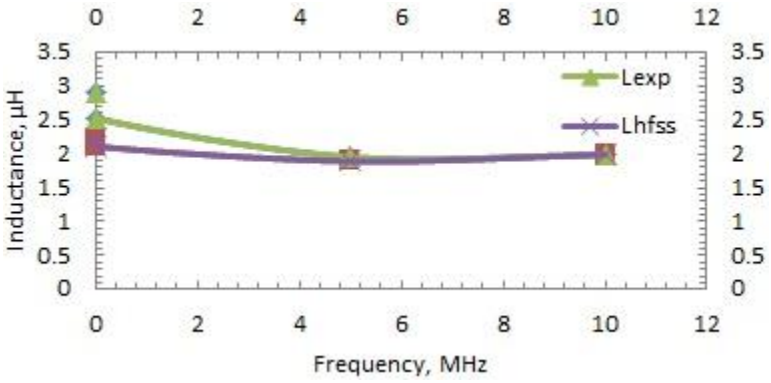


Figure 2.7 Comparison between photolithography fabricated and simulation model

Figure 2.7 shows a plot of inductance vs. frequency for a 7 turn coil with a width (w) = 5 mm and spacing between turns (s) = 5 mm fabricated using photolithography process. The external diameter of the coil ($d_{out}$) = 155 mm and internal diameter ($d_{in}$) = 10 mm. The coil inductance is compared to the inductance of a coil with same parameters modeled using Ansoft HFSS electromagnetic simulation software that makes use of the finite element method to perform simulations.

### 2.4.2 Copper tape method

Using this method, we can make use of a single substrate and easily change the design of the antenna by peeling the copper tape and using another tape with a different design. The steps followed to fabricate planar spiral antennas using this method are:

- The substrate is first made stable by fixing it in a table using tape. The substrate used in this research is kapton. Before making use of kapton substrate, wood was used for preliminary experimental work.

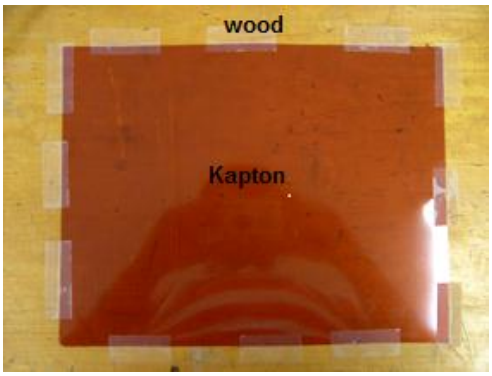


Figure 2.8 Kapton taped on wooden platform

- Copper tape is then taped on top of the substrate. Since the tape is of a particular width, many strips of it are taped to cover the entire substrate. The tapes are attached such that they partially overlap. This overlapping can cause discontinuities which can later be prevented by using solder.

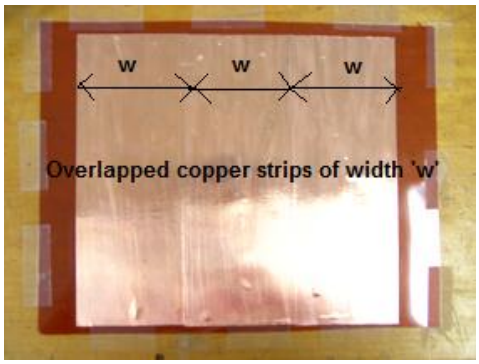


Figure 2.9 Copper strips stuck on kapton substrate

- The mask of the planar spiral antenna made using AutoCAD software [18, 19] is then stuck on the copper tape.

Figure 2.10 Mask taped on copper layer

- An impression is made on the mask along the spiral boundary using a pen knife and then the mask is removed.
- The copper tape is peeled from the substrate to obtain the planar spiral antenna.
- The discontinuities in the coil are then soldered using tin-lead wire.
- The antenna is then tested using an impedance analyzer. If the analyzer shows a negative inductance, the antenna is checked for discontinuities and appropriate connections are made until the analyzer reads positive inductance.

# CHAPTER 3

# ANSOFT HFSS SIMULATION

## 3.1 Finite element analysis

The finite element method (FEM) is a powerful numerical analysis technique which is well-suited to and appropriate for solving a wide variety of electromagnetic applications problems computationally [29]. Amongst the many methods used in computational electromagnetics, its ability to manage problems with complex geometries, as well as its broad applicability to static, quasi-static, wave and transient systems, and to problems containing material regions that are nonlinear, inhomogeneous and anisotropic, all make the FEM one of the most versatile and powerful computational analysis and simulation schemes available today. Moreover, the solid theoretical foundations on which the FEM is based, as well as the rigorous mathematical analysis concerning the existence, convergence, and the uniqueness of finite element solutions that have been established, further justify its use in electromagnetics research and design.

While FEM methods are presently used extensively for electromagnetics analysis and design, the use of adaptive FEM methods has gained considerable attention in recent years from numerical analysts for solving problems more efficiently than standard FEM methods permit. The accuracy of a finite element solution is directly dependent on the number of free parameters used to mathematically represent the problem, and how effectively those parameters, or mathematical DOF(degrees of freedom), are distributed over the problem space. Consequently, the most efficient distribution of DOF for a problem is that which provides a sufficiently accurate solution for the lowest number of free parameters.

Currently, the only practical way to achieve this objective is by using adaptive solution strategies which are capable of intelligently evolving and improving an efficient distribution of

DOF over the problem domain by establishing solution error distributions, and then adjusting or adding DOF to the discretization to correct them. By increasing the number of DOF in the vicinities of higher solution error only, it is possible to make the most significant improvement in the global accuracy of the finite element solution, for the minimum additional computational cost.

## 3.2 Ansoft HFSS simulation

High frequency Structural Simulator (HFSS) is a high performance full wave electromagnetic simulator [13] that employs the finite element method (FEM), adaptive meshing, and brilliant graphics to give insight to 3D electromagnetic problems. Design creation using Ansoft HFSS involves the following -

- Parametric model generation – The geometry of the model is created, the boundaries and excitations are then defined.
- Analysis setup – The solution setup and the frequency sweeps are then defined.
- Results – 2D reports and field plots are then obtained.
- Solve Loop – The solution process is fully automated.

Figure 3.1 is an illustration showing the simulation procedure in Ansoft HFSS.

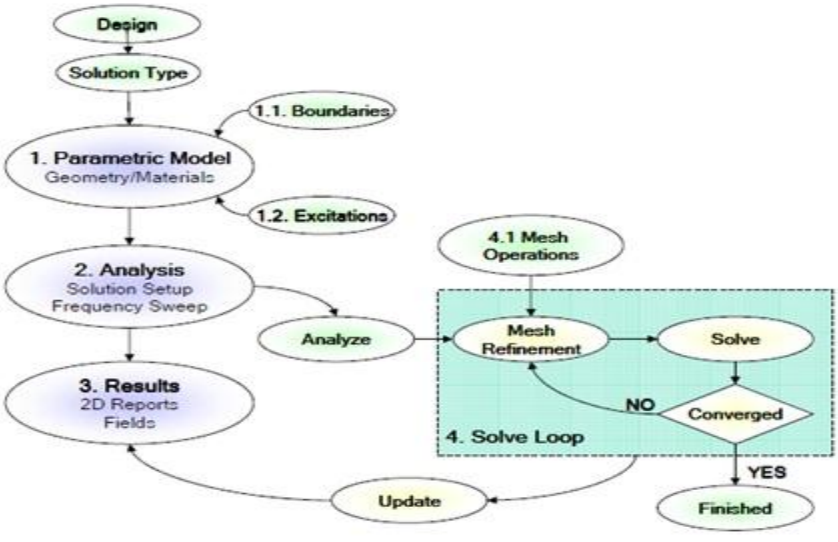


Figure 3.1 Simulation illustration

## 3.3 Sample planar spiral antenna simulation setup

The following steps are involved in creating and simulating a planar spiral antenna -

- To create a new project, we go to File and click on new project. From the project menu, insert HFSS design option is selected.
- Then solution type option from the HFSS menu item is selected and driven terminal solution type is clicked.
- From the 3D modeler menu item, unit's option is selected and the appropriate units are selected.
- The 3D model of planar spiral antenna is then created using the HFSS graphical user interface. Boundary conditions are applied and internal ports (lumped ports) are assigned to the model. Care is taken that appropriate material properties are assigned to different parts of the model.
- From the HFSS menu option, analysis setup is selected and Add solution setup sub option is then selected. The solution frequency, the maximum number of passes, and the maximum error between each pass is then defined.
- From the HFSS menu option, Analysis Setup is selected and Add sweep sub option is then selected. The start frequency, stop frequency and the sweep type which is usually interpolating is then selected.
- The file is then saved and the validation check option from the HFSS menu option is then selected to ensure whether there are any errors or not in the simulation setup.
- The Analyze All option from the HFSS menu option is then selected. The simulation then begins and ends when the solution converges.
- From the HFSS menu option, the results option is selected and the create report sub option is then selected.

- The formulas for inductance and quality factor for the antenna are then inputted. $L = \frac{\mathrm{Im}(\frac{1}{Y_{11}})}{(2 * pi * freq)}$ & $Q = \frac{\mathrm{Im}(\frac{1}{Y_{11}})}{\mathrm{Re}(\frac{1}{Y_{11}})}$. These formulas [15, 28] are in the y axis of the curve that is plotted with the x axis as frequency. The results are then exported in an excel format and the values are obtained for frequency of interest.

A sample planar spiral inductor modeled using Ansoft HFSS is shown below –

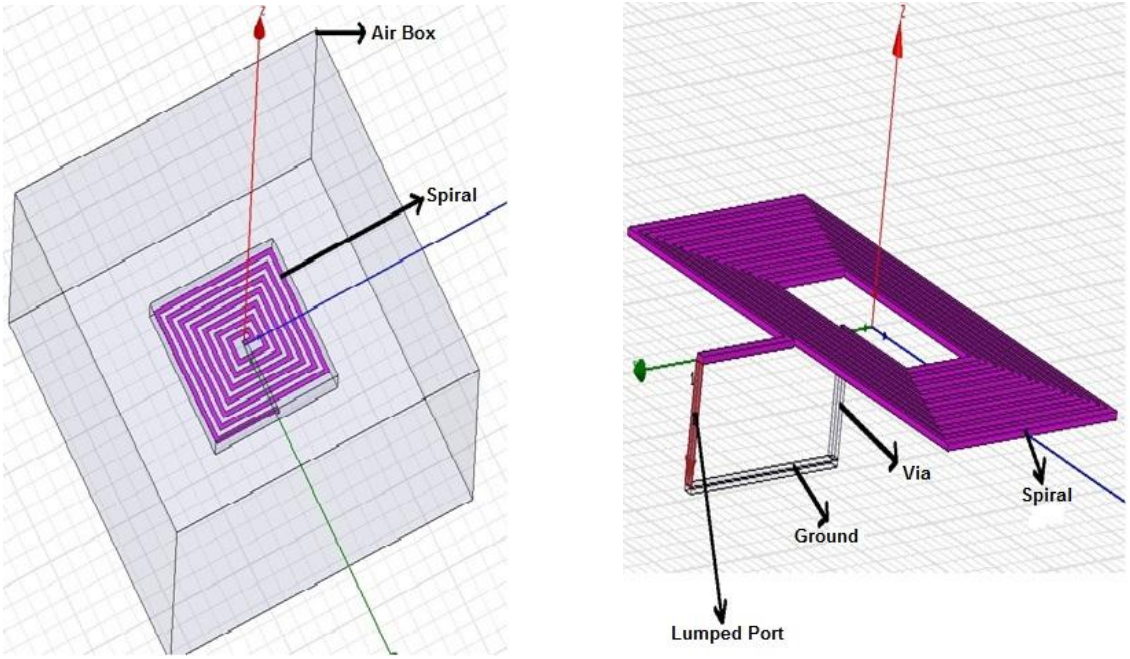


(a) (b)

Figure 3.2 (a) Top view and (b) Side view of simulation model

## 3.4 Matching simulations with equations

Different designs of planar antennas were implemented in order to confirm the validity of the equations in [17] with the simulation results. Since, it is clearly mentioned in [17] that the

inductance equations are only valid for dc frequencies; antennas with different designs were simulated for different number of turns and for different dc (less than 800 kHz) frequencies.

Shown in Figure 3.5 is an antenna with a turn spacing and width of 8 mm, thickness of 0.1 mm and an external diameter of 15 mm. An FR4 substrate of size 30 mm x 30 mm was used in simulation.

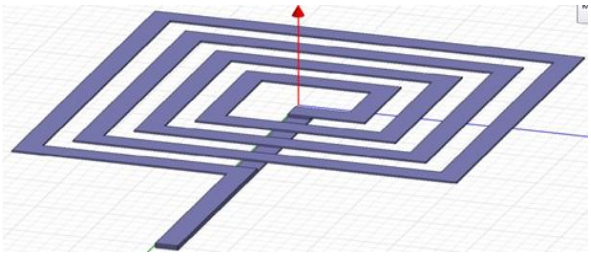

Figure 3.3 HFSS spiral antenna model

Simulations were carried out for 500 KHz, 1 MHz, 1.3 MHz, 5 MHz and 10 MHz frequencies. The values $L_{mw}$ and $L_{gmd}$ are inductance values obtained from formulas in [17]. The value $L_{hfss}$ is obtained from simulations performed in this research. As the frequency increases, it is observed that the deviation of the three inductances increases from each other. This validates the fact, that the inductance values $L_{mw}$ and $L_{gmd}$ are only valid for dc frequencies.

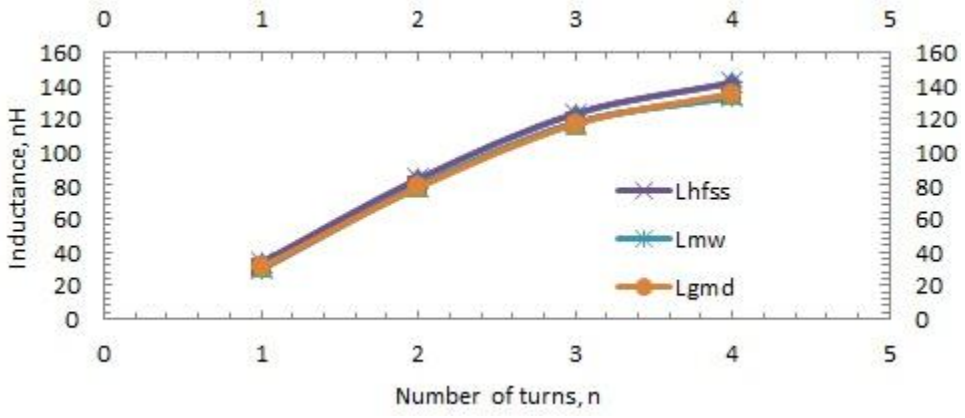


Figure 3.4 Simulation result for 500 kHz frequency

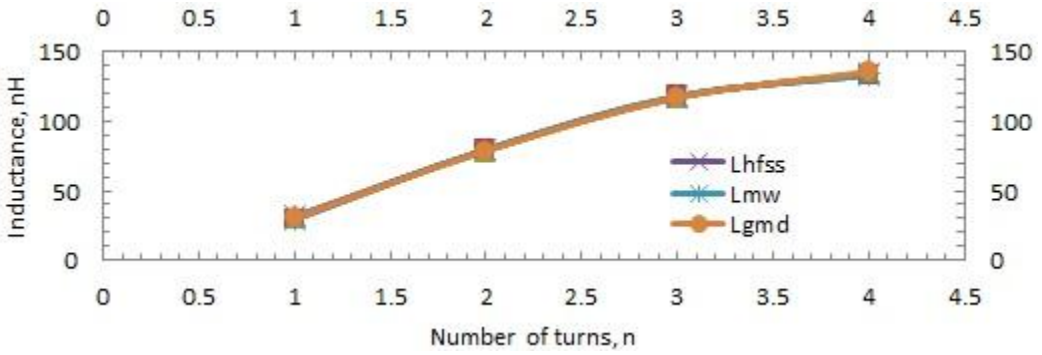


Figure 3.5 Simulation result for 5 MHz frequency

Shown in Figure 3.6 is another design of an antenna where the turn spacing and width are equal to 0.2 mm and the thickness is equal to 0.1 mm. The external diameter of the antenna is 50 mm. The substrate size is 100 mm x 100 mm and thickness is 1.5 mm. The graphs shown in Figure 3.8 and Figure 3.9 also show the deviation of the three inductances with the increase in frequency.

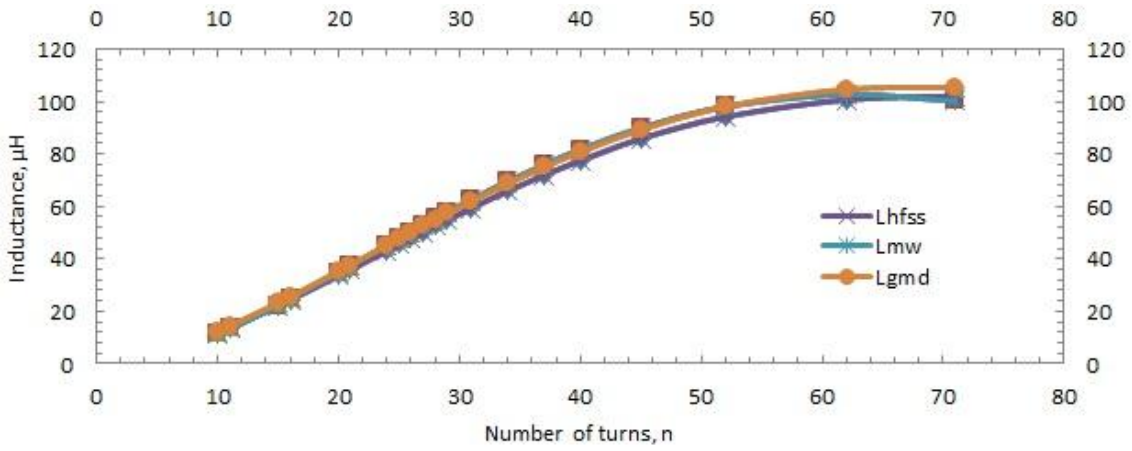


Figure 3.6 Simulation result for 500 kHz frequency

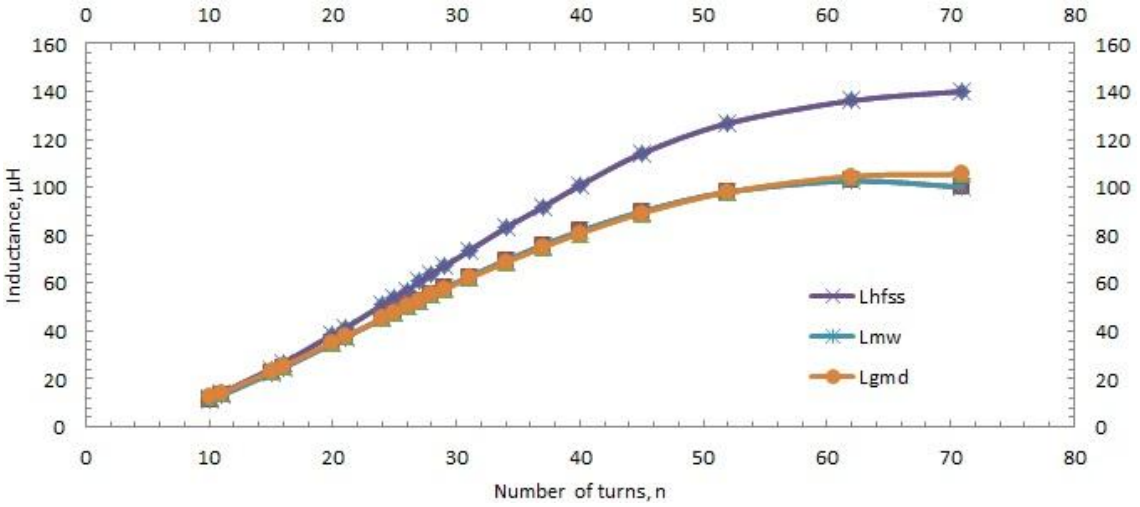


Figure 3.7 Simulation result for 5 MHz frequency

## 3.5 Matching simulations with publications

In order to ensure that the simulations performed using Ansoft HFSS are correct, Several IEEE papers [25, 26, 27] were implemented and the HFSS results obtained from simulations carried out in research work were matched with the HFSS results obtained from the IEEE papers. Figure 3.10 shows the results obtained from [24].

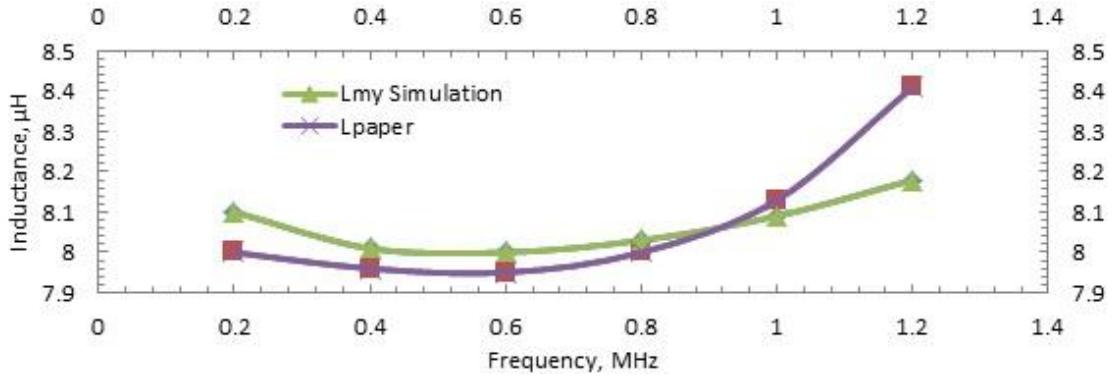


Figure 3.8 Publication [24] Vs. Simulation result

Here the values $L_{my\ Simulation}$ and $L_{paper}$ are the inductances of the model implemented in this research and the author. There is a small variation in the results between the simulation by

these authors and this research simulation, this can be explained by the different software versions used and the size of the radiation boundaries.

HFSS simulations were also implemented to match results in another paper [16]. The graphs showing research results and those in [16] are shown in Figure 3.11. This time the results being matched are the quality factor of the coils.

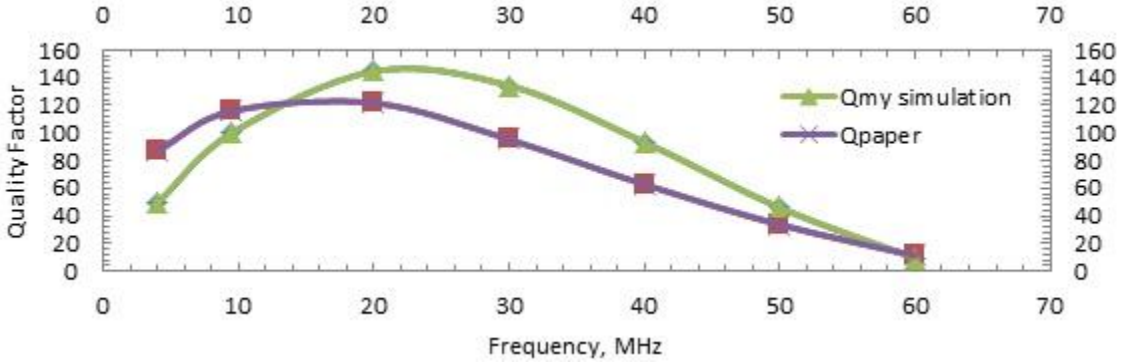


Figure 3.9 Publication [16] Vs. Simulation result

Here the values $Q_{my\ simulation}$ and $Q_{paper}$ are the quality factors obtained from HFSS implementation and the implementation by [16]..

## 3.6 Matching simulations with experiments

The HFSS simulations were later matched with experiments. Different experiments were run using antennas of different design and on different substrates. The results of which are shown below. A 7 turn antenna of thickness 0.035 mm, turn and spacing width 5 mm is fabricated on a 13.5 mm thick wooden substrate using the copper tape method. The $L_{mw}$ and $L_{gmd}$ values of this antenna are 3.384 and 3.4975 micro-henry respectively. A picture of the antenna is shown below. The value $L_{exp}$ of the antenna is obtained after subtracting the probe inductance from the inductance obtained using the LCR meter.

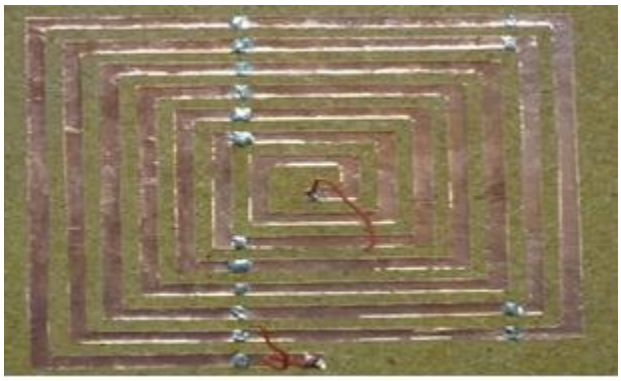

Figure 3.10 Spiral antenna fabricated on a wooden substrate

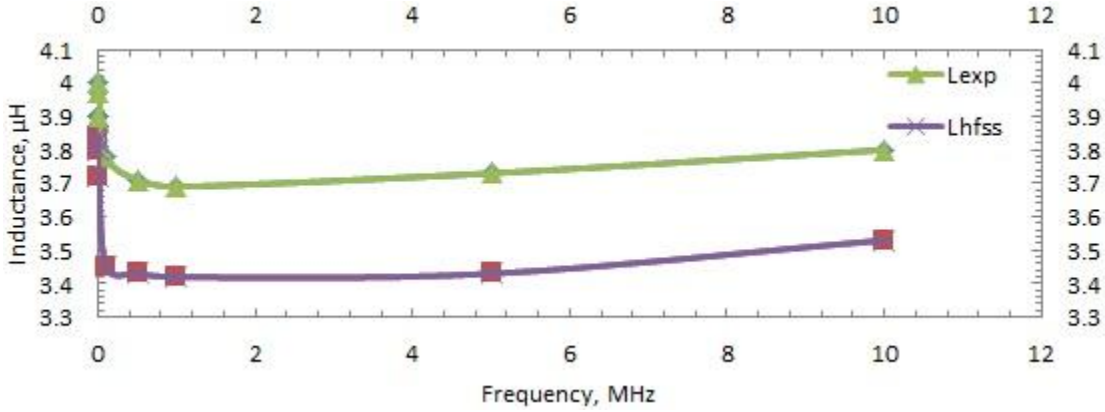


Figure 3.11 Comparison result between simulation and coil fabricated on wooden substrate

Antenna with the Figure 3.12 design is then fabricated on kapton substrate using Copper tape method.

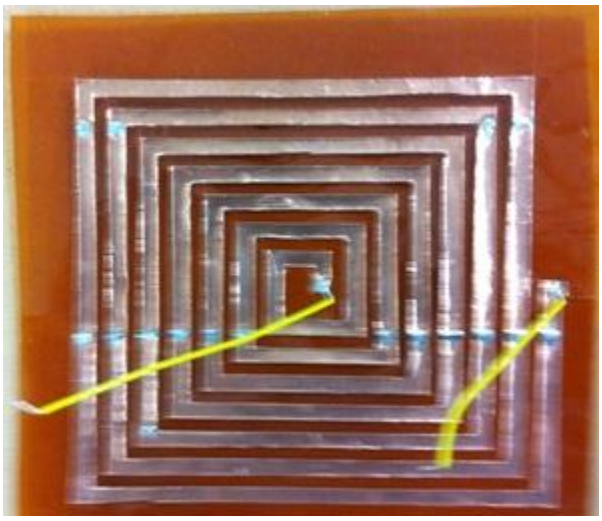

Figure 3.12 Spiral antenna fabricated on kapton substrate

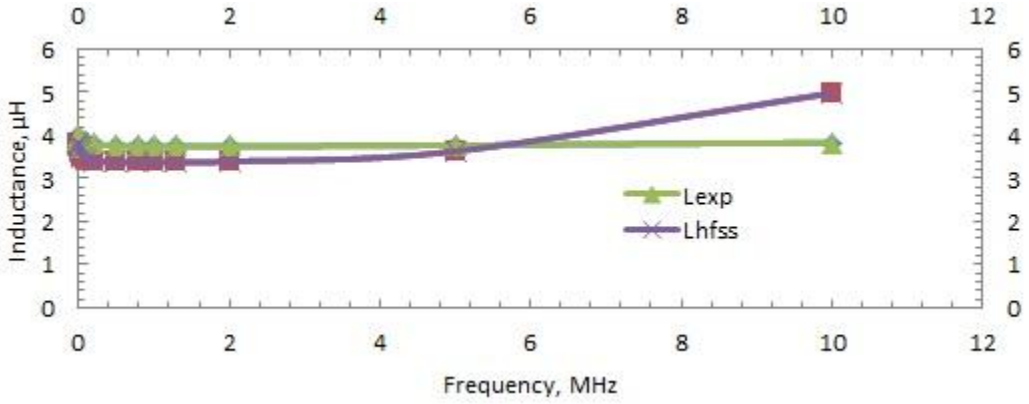


Figure 3.13 Comparison result between simulation and coil fabricated on kapton substrate

A 14 turn planar spiral antenna is then fabricated on a wooden substrate of thickness 13.5 mm. The turn and spacing width of the antenna is 5 mm and the thickness of the copper coil is 0.035 mm. The fabrication is performed using copper tape method. HFSS simulations and measurements are then performed for different turns and the results are compared.

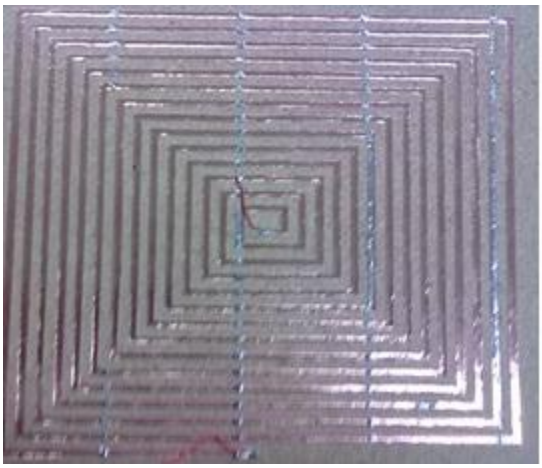

Figure 3.14 Spiral antenna on wooden substrate with n=14, $L_{mw}$ = 2.2388 µH, $L_{gmd}$ = 2.5285 µH

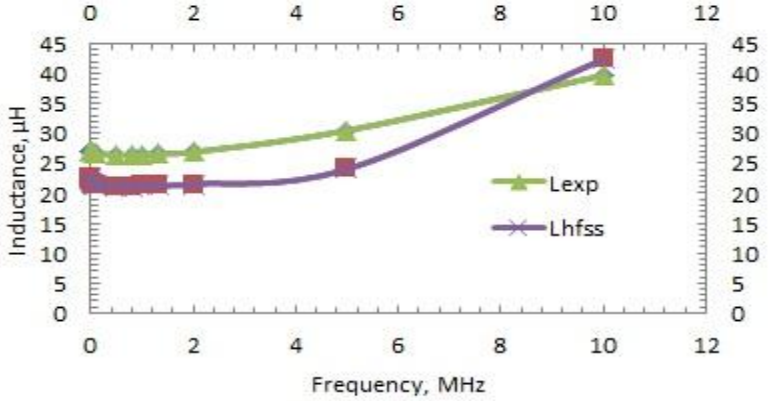


Figure 3.15 Comparison result between 14 turn coil and corresponding simulation model

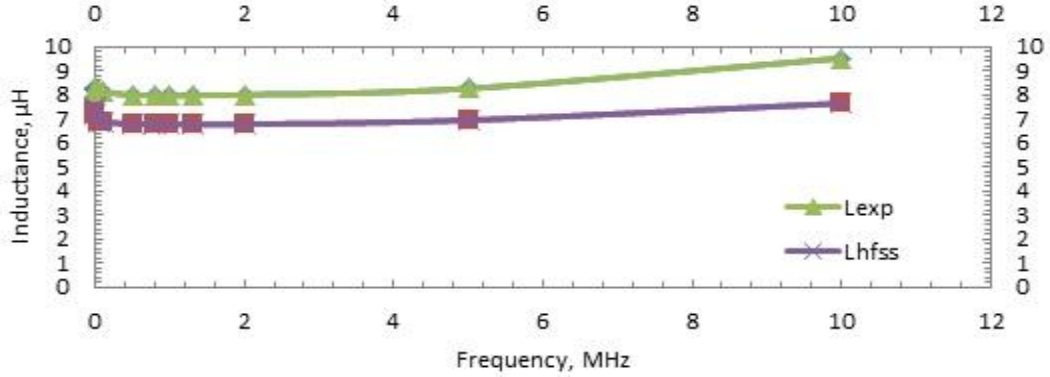


Figure 3.16 Comparison result for n=9, $L_{mw}$ = 6.8542 µH, $L_{gmd}$ = 7.1112 µH

## 3.7 Matching simulations with bent antenna

The coil antenna is fabricated on a flexible substrate in order to provide comfort to the patient who is wearing it. Since a bent coil is used, simulation has to be also performed in HFSS for bent coils. Since HFSS does not provide a method to bend the coil, the coil model has to be exported to a format that can be used by a different program that allows for a bent substrate to bend it. AutoDesSys Inc. provides software called Bonzai 3d that can be used to bend the coil along any plane and to any degree. After bending the coil, the bent coil model can be exported to a format that can be imported into HFSS for performing simulations.

After modeling the coil in HFSS, the model can be exported in .sat format. The (.sat) file can later be imported into Bonzai 3d software [20].The software has a bend function that can be used to bend the coil antenna to any degree and along XY, YZ or XZ axis. In this case the model was bent along XZ axis. The bent coil model is then exported in .sat (standard ACIS text) format. The file is then imported into HFSS and after applying boundary conditions, excitations, the simulation is then started. A sample 7 turn coil model is simulated after being bent and the results are compared to experimental results.

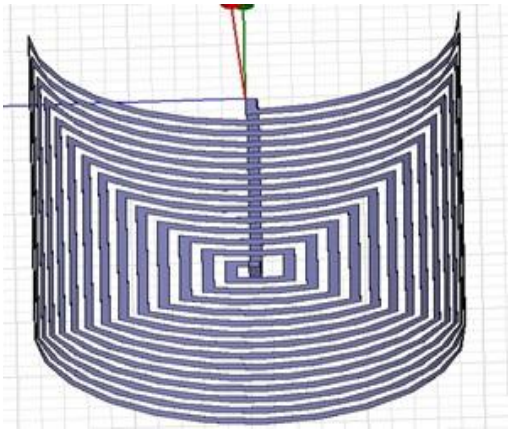

Figure 3.17 Top view of bent antenna model

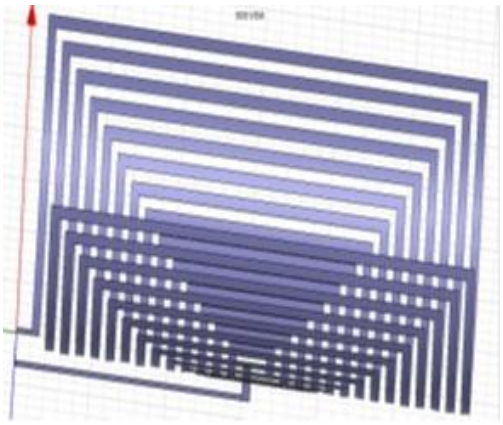

Figure 3.18 Side view of bent antenna model

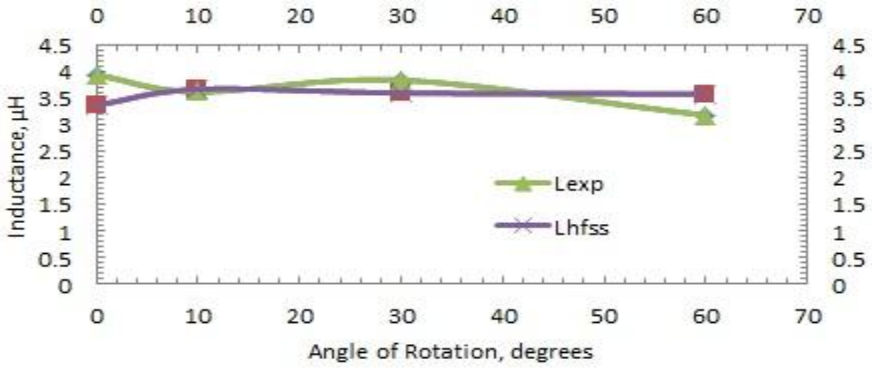


Figure 3.19 Comparison result at 1.3 MHz between simulation and experiment

CHAPTER 4

FLEXIBLE ANTENNA EXPERIMENTS

The efficiency pattern of the flexible antenna is obtained using a Class – E power amplifier circuit [5, 9, 11], a receiver circuit, and a well, designed setup which ensures the stability and repeatability of all experiments conducted using the setup.

## 4.1 Class-E power amplifier circuit

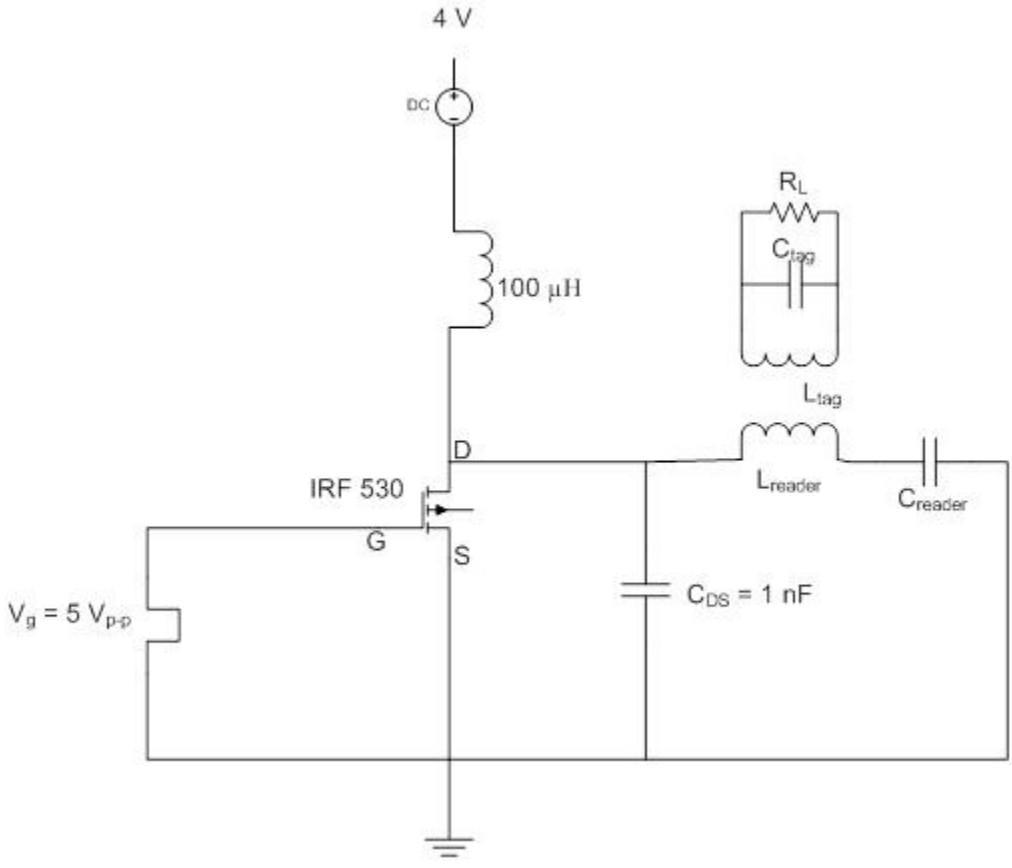


Figure 4.1 Class – E amplifier circuit

Class – E amplifiers can operate with power losses smaller by a factor of 2.3 [11] compared with conventional Class – B or Class - C amplifiers making use of the same transistor at the same frequency and output power. Class – E power amplifiers also have a very high efficiency compared to other conventional amplifiers. Hence, it is used in this experimental work described in this thesis. Also the MOSFET used is IRF 530 (enhancement type N channel MOSFET), because it has a low threshold voltage and has a higher efficiency as compared to IRF 510 transistor.

The amplifier operates as follows. The 100 μH inductor connected at the drain acts as a constant current source. When the switch closes, $L_{Reader}$ supplies current through the switch and no current flows through $C_{DS}$. When the switch opens, the inductor supplies current through $C_{DS}$ and no current flows through the switch thereby building a voltage across the switch. The amplifier operation is such that the voltage and current at the switch have a phase difference of 90 degrees at all times. This results in very low power losses and high efficiency of the amplifier. There is a particular value of $C_{Reader}$ and $C_{Tag}$ at which the amplifier resonates at 1.3 MHz frequency and the efficiency of power transfer between the $L_{Reader}$ and $L_{Tag}$ through the resonant magnetic coupling phenomenon, is maximum. Care is always taken that resonance is achieved before obtaining the efficiency patterns for any of the antenna characterization configurations so that stability and hence repeatability of the experiments is ensured.

The efficiency of power transfer between the two coils is calculated based on equations (4.1) – (4.3).

$$P_i = V_{DD} \times I_{DD} \tag{4.1}$$

where $P_i$ is the input power and the dc voltage $V_{DD}$ is fixed at 4 V.

$$P_o = \frac{V^2}{R_{Load}} = \frac{V^2}{500} \tag{4.2}$$

where $V$ is the voltage across the load resistor and $P_o$ is the output power delivered to the load.

The efficiency of power transfer is then calculated using (4.3).

$$\eta \text{ In \%} = \frac{P_O}{P_i} \times 100\% . \quad (4.3)$$

## 4.2 Introduction to experiments

Four different experiments are performed to characterize the flexible antenna.

- Antenna misalignment – The tag antenna is fixed and the reader antenna is rotated along a particular curvature. The angle at which both the reader antenna and tag antenna are center aligned is considered 0 degrees. The clockwise rotation of the reader antenna is considered positive rotation and the anticlockwise rotation of the reader antenna is considered negative rotation. A graph is obtained with the reader antenna angular rotation plotted along the x axis and the efficiency values at the corresponding reader antenna positions plotted along the y axis. The experiment is repeated for all 3 different curvatures of the reader antenna and at tag antenna distances of 4 cm, 6 cm and 8 cm from the reader antenna.
- Antenna pattern - The reader antenna is fixed and the tag antenna is rotated along its axis. The angle at which both the reader antenna and tag antenna are center aligned is considered 0 degrees. The clockwise rotation of the tag antenna is considered positive rotation and the anticlockwise rotation of the tag antenna is considered negative rotation. A graph is obtained with the tag antenna angular rotation plotted along the x axis and the efficiency values at the corresponding tag antenna positions plotted along the y axis. The experiment is repeated for all 3 different curvatures of the reader antenna and at tag antenna distances of 4 cm, 6 cm and 8 cm from the reader antenna.
- Cross section pattern – The reader antenna is fixed and the tag antenna is moved upwards and downwards with the distance between the two antennas fixed. The

position at which both the reader antenna and tag antenna are center aligned is considered the origin. The upward movement of the tag antenna is considered negative movement from the origin and the downward movement of it is considered positive movement from the origin. A graph is plotted with tag antenna movement from the origin, along the x axis and the efficiency values at the corresponding tag antenna positions along the y axis. The experiment is repeated for all 3 different curvatures of the reader antenna and at tag antenna distances of 4 cm, 6 cm and 8 cm from the reader antenna.

- 3D pattern – To perform the experiment two acrylic plates are used. The reader antenna is fixed in the reader plate using tape. A tag antenna plate is made by making a 26 cm x 26 cm square pattern of holes spaced 1 cm apart. The tag antenna is moved along these holes at distances of 2 cm apart and the efficiency of power transfer is measured. At the end the efficiency pattern is obtained for 13 cm x 13 cm square matrix. The reader antenna is fixed and the tag antenna plate is moved at distances of 4 cm, 6 cm and 8 cm from the reader antenna plate and the efficiency pattern is obtained. For references and efficiency pattern plotting, two axis – the x axis and y axis are used. The vertical upward and downward movement of the tag antenna in the tag antenna plate is considered negative and positive movement of the tag antenna along the x axis. The horizontal east and west movement of the tag antenna is considered positive and negative movement of the tag antenna along the y axis.

## 4.3 Antenna characterization setup requirements

In order to obtain an accurate characterization [12] of an antenna, the following steps need to be taken.

The system needs to be very stable. This can be realized by building a system that requires the least human intervention. The setup should be such that, the reliability of the measurements should be maintained. Hence the experiments performed should be repeatable. The setup

should be small and easy to handle to promote ease of experiments with minimum errors. This would require the setup to be reconfigurable. The setup should be such that, a large number of readings from the setup can be taken in a short interval of time. Unnecessary hardware components should be removed to reduce hardware costs. A better measurement sensitivity capability should be maintained in order to obtain experimental accuracy.

## 4.4 Experimental setup design

In order to realize such a system, where the above conditions are met, a design was made and was accurately fabricated using a CNC machine. The design of the setup for one groove is shown in Figure 4.2.

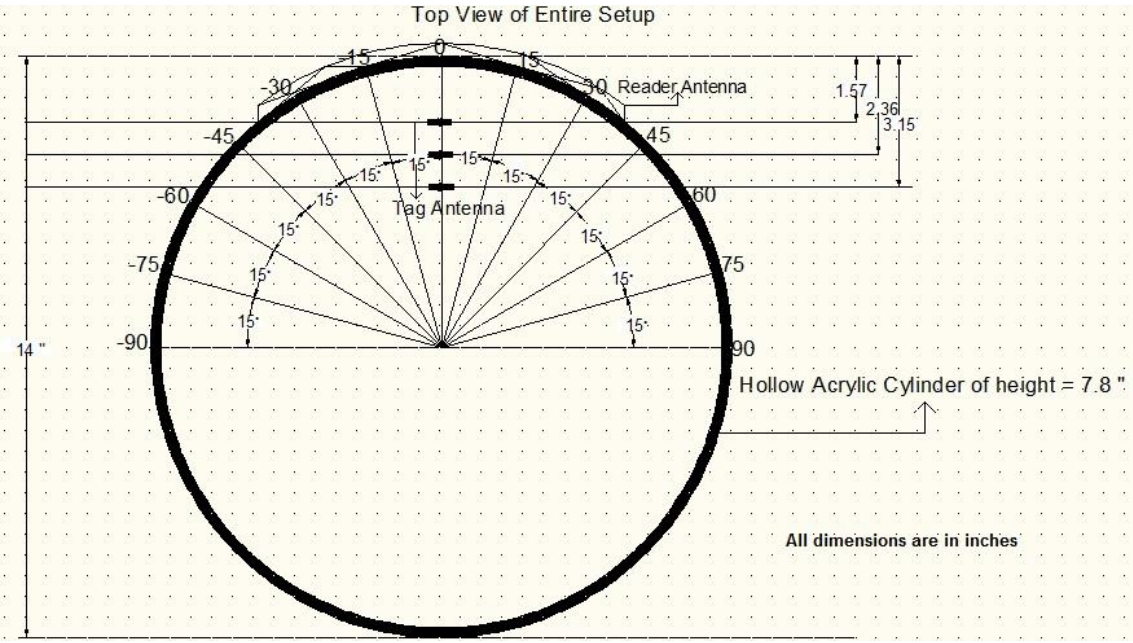


Figure 4.2 Top view of entire setup with a schematic of rotation angle of reader antenna

In order to make the setup reconfigurable and, as per the dimensions mentioned in Figure 4.3, three grooves were made of diameters equal to the diameters of 3 pvc pipes. Three holes were made at distances 4 cm, 6 cm and 8 cm from the 0 degree position (origin) mentioned in Figure 4.2. These holes were made to fit the acrylic stick into which tag antenna would be fixed using tooth pick and tape. A schematic of the three grooves and holes is shown in Figure 4.3.

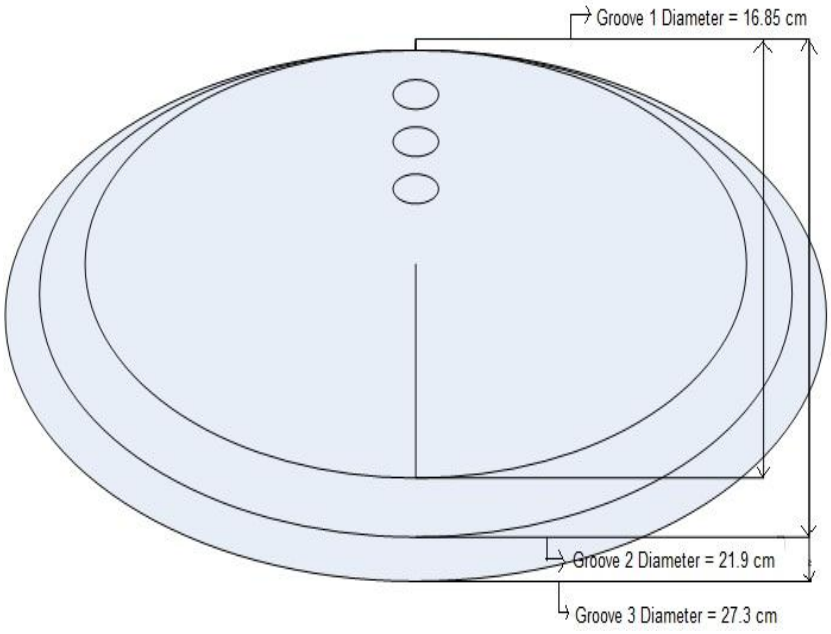


Figure 4.3 Reconfigurable setup schematic

The pvc pipe is cut into half for ease in performing experiments. The reader antenna is stuck behind the pvc pipe which is made to fit into the respective groove and the experiments are performed. Antenna misalignment, antenna pattern and cross section pattern are then obtained as shown in Step 1, Step2 and Step3 of Figure 4.4.

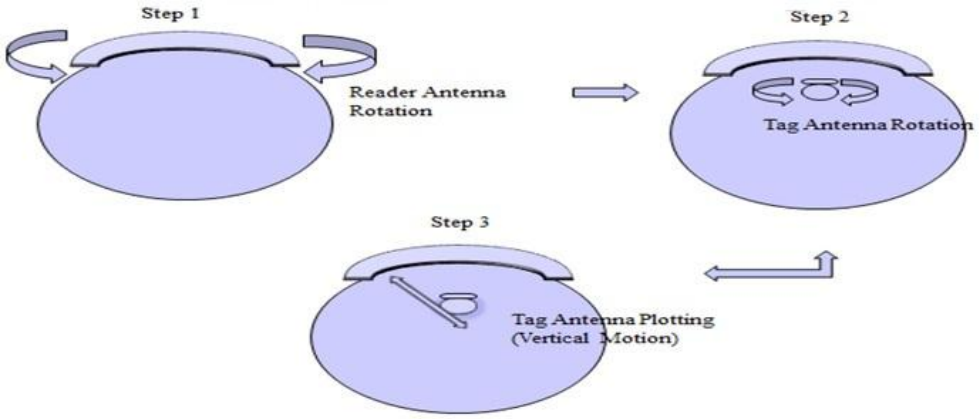


Figure 4.4 Antenna misalignment, Antenna pattern, Cross section pattern using steps – 1, 2, 3

The 3D pattern is obtained using the setup design shown in Figure 4.8.

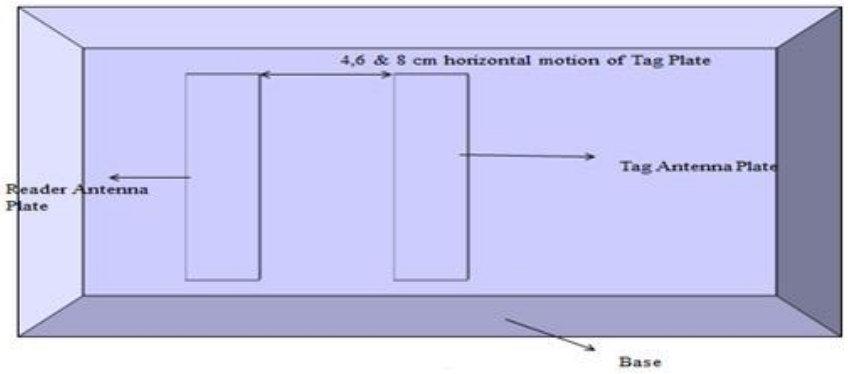


Figure 4.5 3D pattern setup design

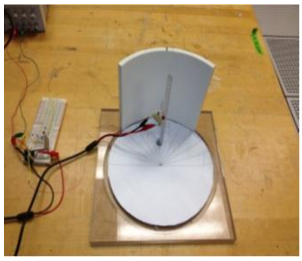

(a)

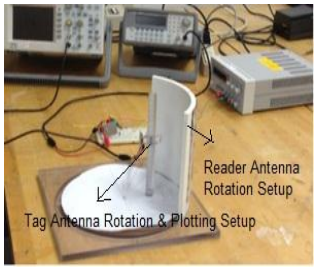


(b)

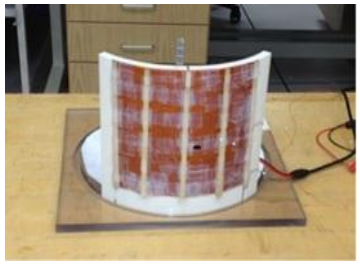

(c)


(d)

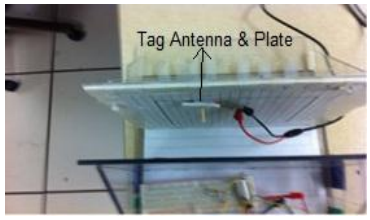


(e)

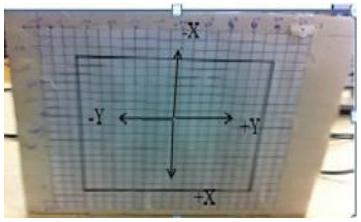


(f)

Figure 4.6 (a) Top view, (b) Side view of setup, (c) Back view of pvc where reader antenna is attached, (d) Top view of 3D setup, (e) Top view of 3D setup, (f) Front view of tag antenna plate

## 4.5 Experiment parameters

After achieving a good experimental set up, experiments were conducted and the parameters used are discussed. Experiments were conducted using three curvatures C1 of radii = 8.4 cm, C2 of radii = 11 cm and C3 of radii = 14 cm. As discussed before, three half sections of pvc pipes were used to emulate the bend. Based on the radii C1 had the highest bend, C2 had the second highest bend, and C3 had the least bend. Antennas with two different designs were used in the experiments. Since with bending of the coil, antenna inductance reduces and the transmitter circuit had to be retuned for each bend [7, 8]. The receiver circuit is changed only once when tuning the antenna for the first time when it is straight. There after only the transmitter circuit is retuned. Also the two antennas are abbreviated as A1 and A2. The component parameters are mentioned in Table 4.1.

| Parameters | A1 | A2 |
|---|---|---|
| $L_{reader}$ (μH) | 20.69 | 28.97 |
| $L_{tag}$ (μH) | 35.37 | 35.37 |
| Number of turns | 16 | 18 |
| Spacing (mm) | 2 | 2 |
| Width (mm) | 3 | 3 |
| Thickness of turns (mm) | 0.035 | 0.035 |
| Antenna Shape | Square | Square |
| Creader for Straight Curvature (pF) | 775 | 675 |
| Creader for Curvature C1 (pF) | 796 | 705.4 |
| Creader for Curvature C2 (pF) | 792 | 697.1 |
| Creader for Curvature C3 (pF) | 790 | 684.2 |
| $C_{tag}$ (pF) | 300 | 300 |

Table 4.1 Experiment parameters

## 4.6 Antenna characterization results

Legends shown in the graphs of Figure 4.7 – Figure 4.26 and Figure 4.30 – Figure 4.49, consists of 4 parts separated by commas. The first part is the antenna used – A1 or A2. The second part is the curvature used – C1, C2, C3 or St (straight). The third part is the distance between the reader coil and tag coil. The fourth part is the experiment conducted – A.M (Antenna Misalignment), A.P (Antenna Pattern), C.P (Cross-section Pattern) and 3D.P (3D Pattern).

Results obtained using Antenna 1 are shown in Figure 4.7 – Figure 4.29.

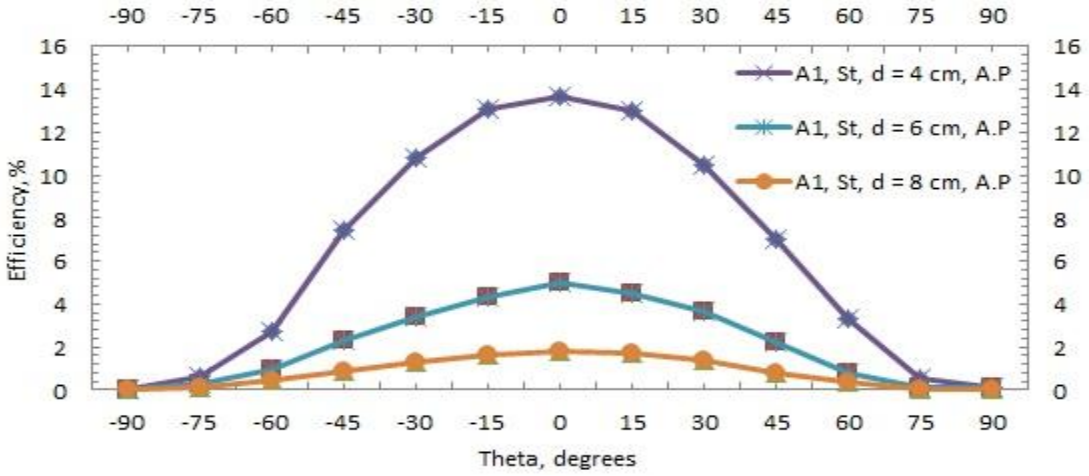


Figure 4.7 Antenna pattern distance comparison for A1 with flat bend

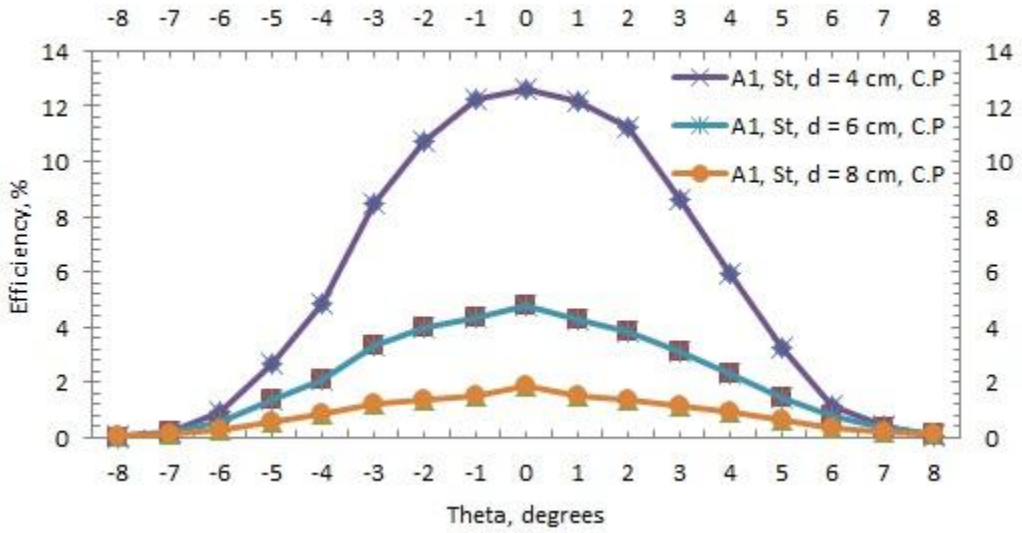


Figure 4.8 Cross-section pattern distance comparison for A1 with flat bend

The maximum efficiency obtained using the straight reader antenna is around 12 - 13 % when the two coils are center aligned. From the comparison graphs, it is observed that the efficiency reduces with distance. The efficiency pattern has a gaussian shape for misalignment pattern, antenna pattern and cross section pattern experiments. The graphical results for the least bend curvature i.e. C3 are shown in Figure 4.9 – Figure 4.11.

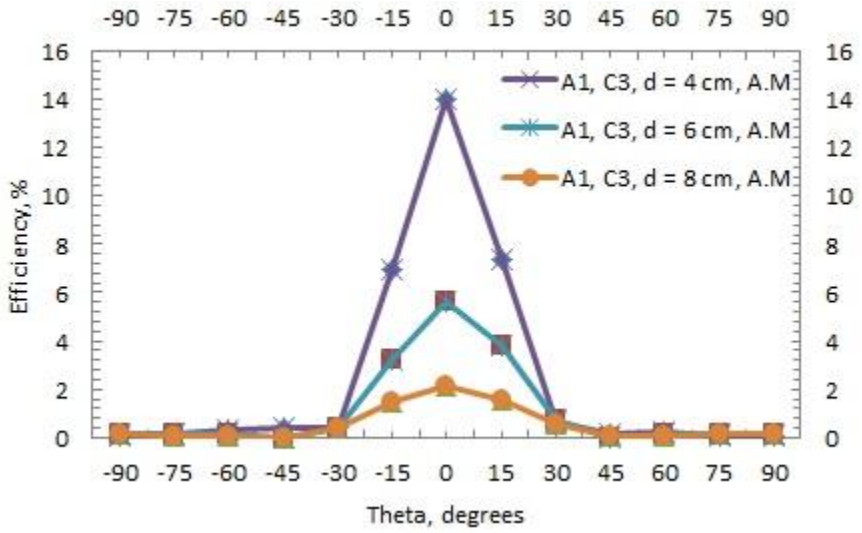


Figure 4.9 Antenna misalignment distance comparison for A1 with C3 bend

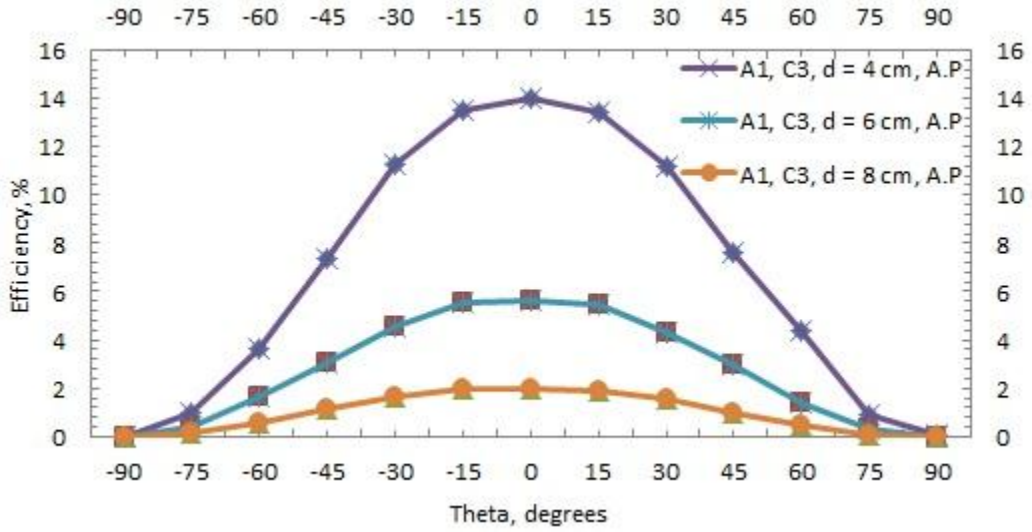


Figure 4.10 Antenna pattern distance comparison for A1 with C3 bend

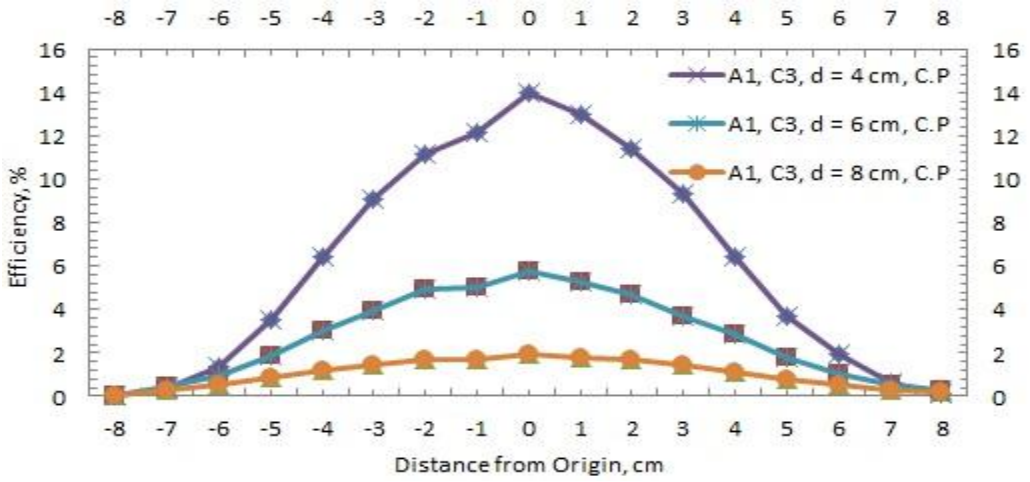


Figure 4.11 Cross-section pattern distance comparison for A1 with C3 bend

The maximum efficiency obtained with the reader antenna bent at C3 with the two coils center aligned increases to around 14 %. From the comparison graphs, it is observed that the efficiency reduces with distance. The efficiency pattern has a gaussian shape for misalignment pattern, antenna pattern and cross section pattern experiments. The graphical results for the C2 bend are shown in Figure 4.12 – Figure 4.14.

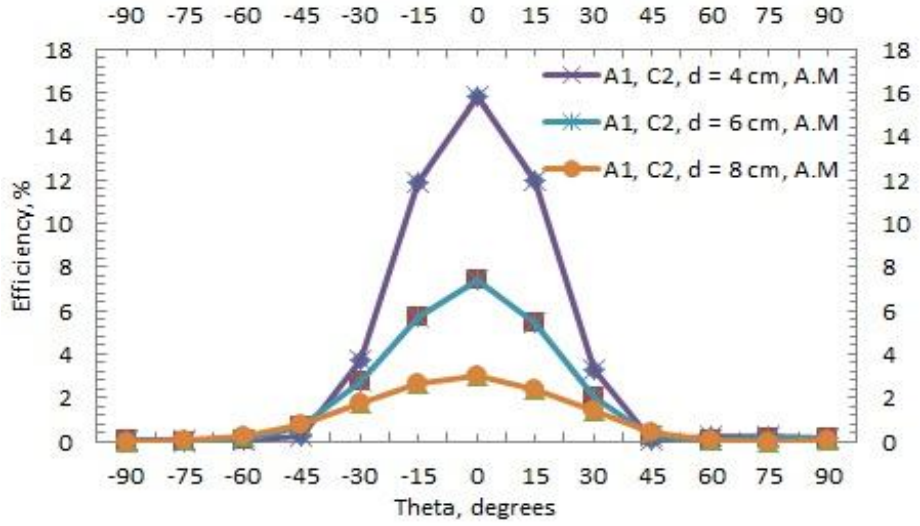


Figure 4.12 Antenna misalignment distance comparison for A1 with C2 bend

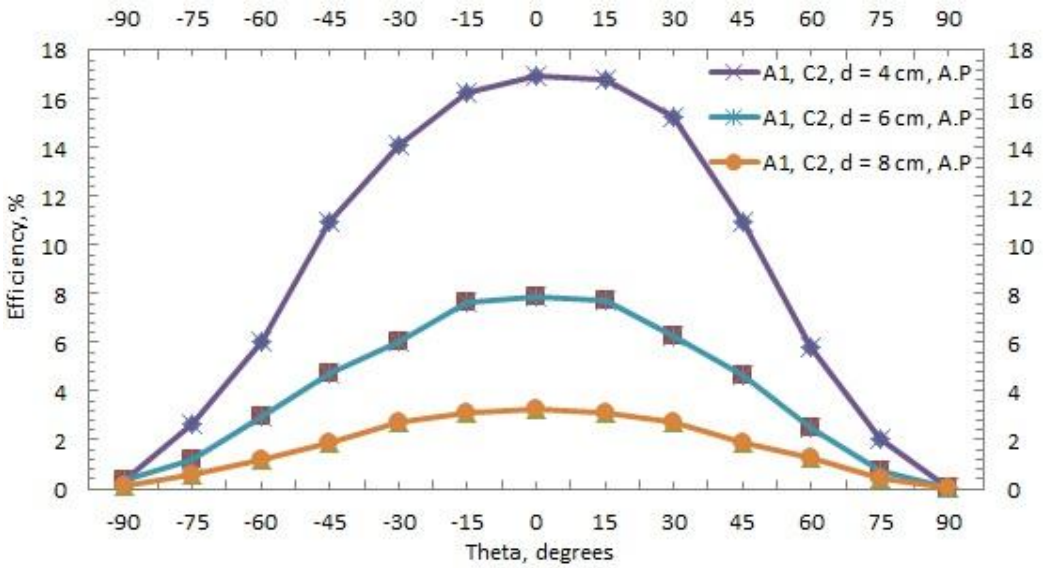


Figure 4.13 Antenna pattern distance comparison for A1 with C2 bend

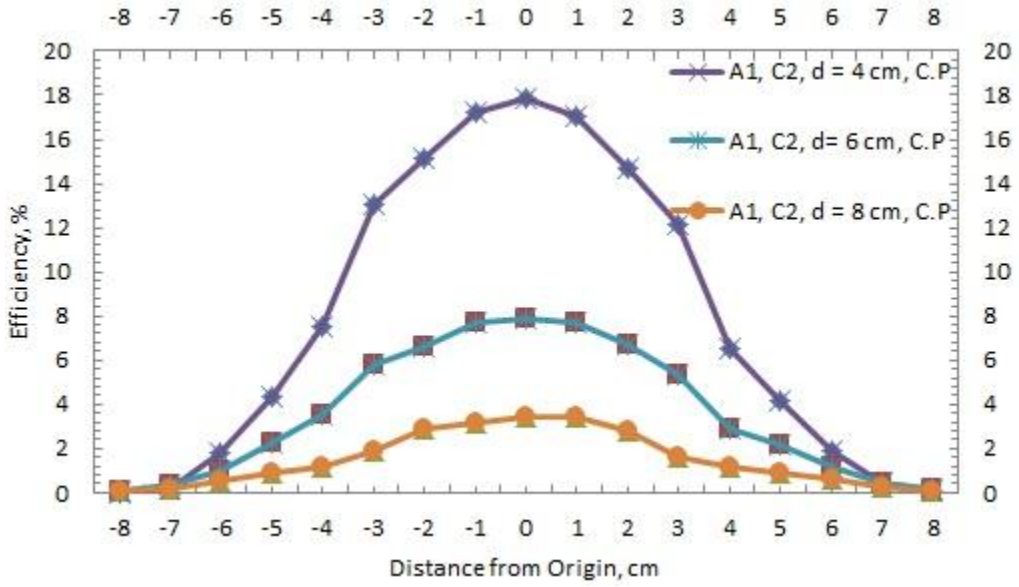


Figure 4.14 Cross-section pattern distance comparison for A1 with C2 bend

The maximum efficiency obtained with the reader antenna bent at C2 with the two coils center aligned increases to around 16 % - 17 %. From the comparison graphs, it is observed that the efficiency reduces with distance which can be explained from inverse square law. The efficiency pattern has a gaussian shape for misalignment pattern, antenna pattern and cross

section pattern experiments. The graphical results for C1 bend is shown in Figure 4.15 – Figure 4.17.

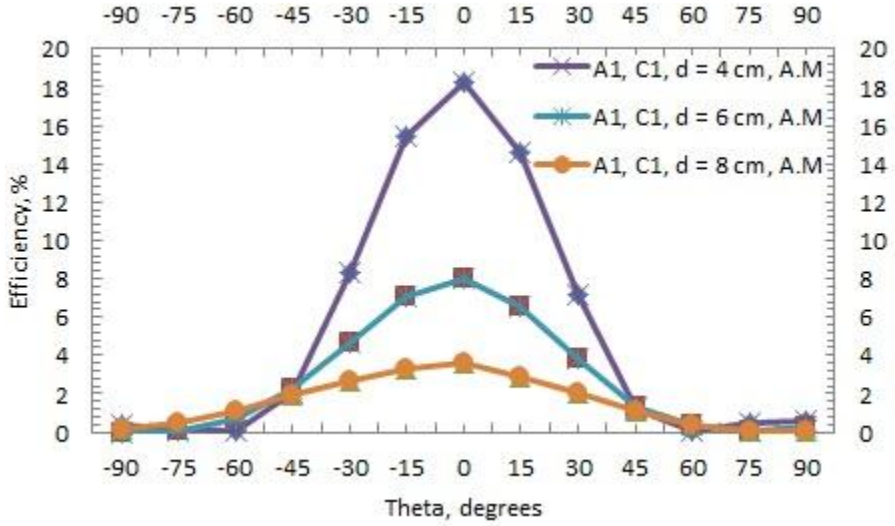


Figure 4.15 Antenna misalignment distance comparison for A1 with C1 bend

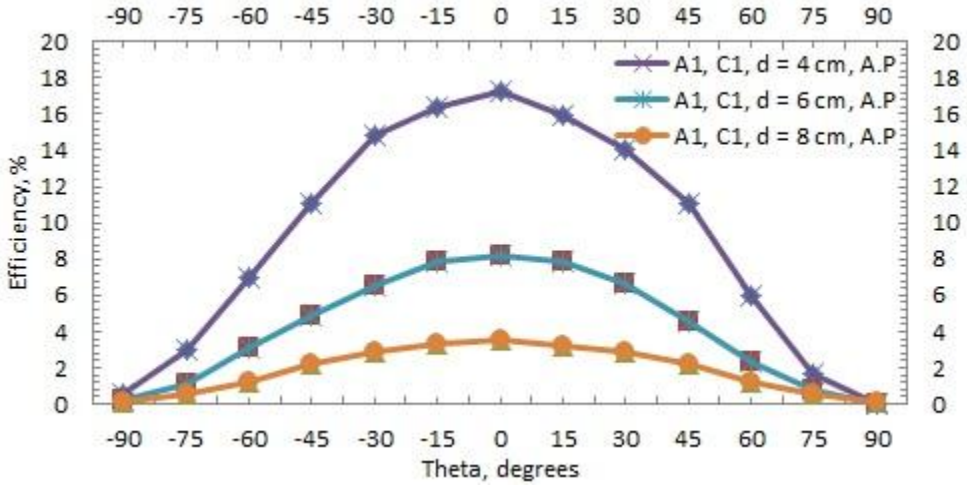


Figure 4.16 Antenna pattern distance comparison for A1 with C1 bend

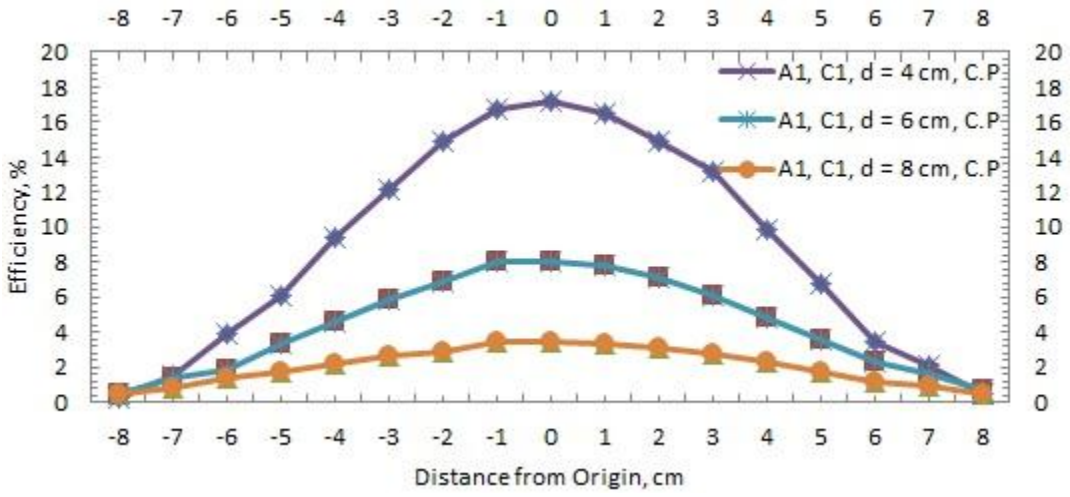


Figure 4.17 Cross-section pattern distance comparison for A1 with C1 bend

The maximum efficiency obtained with the reader antenna bent at C1 with the two coils center aligned is around 18 %. From the comparison graphs, it is observed that the efficiency reduces with distance. The efficiency pattern has a gaussian shape for misalignment pattern, antenna pattern and cross section pattern experiments. Graphs of different curvatures are then compared keeping the parameter, distance as constant.

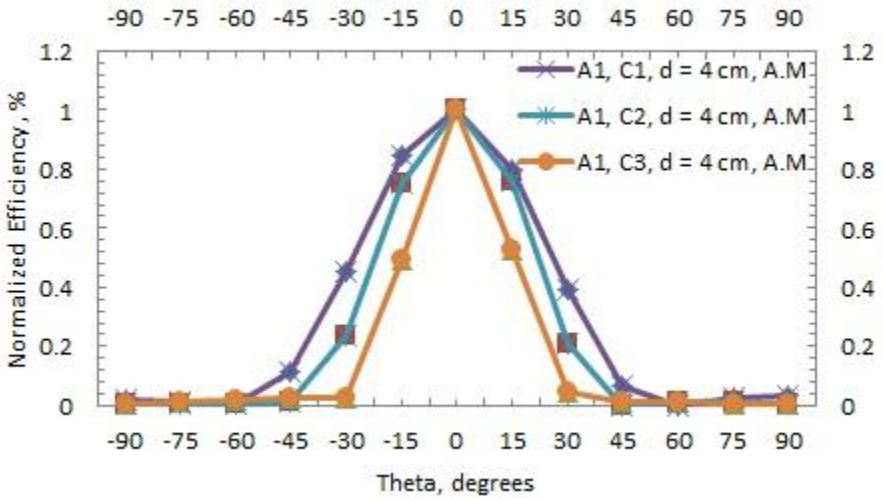


Figure 4.18 Antenna misalignment curvature comparison for A1 at 4cm distance

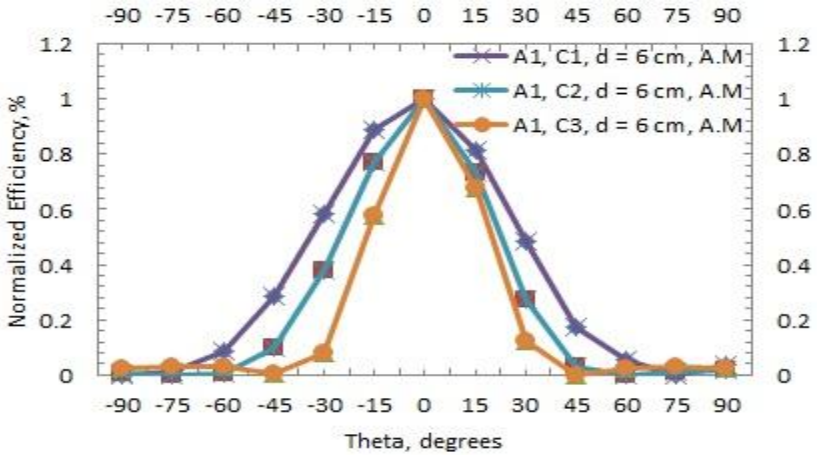


Figure 4.19 Antenna misalignment curvature comparison for A1 at 6 cm distance

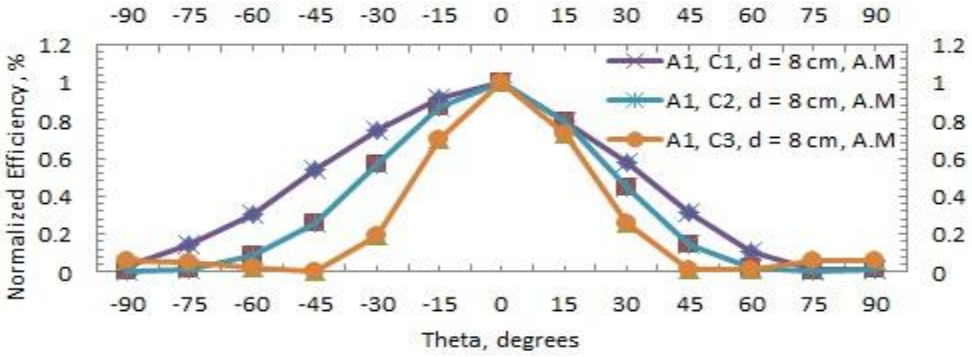


Figure 4.20 Antenna misalignment curvature comparison for A1 at 8 cm distance

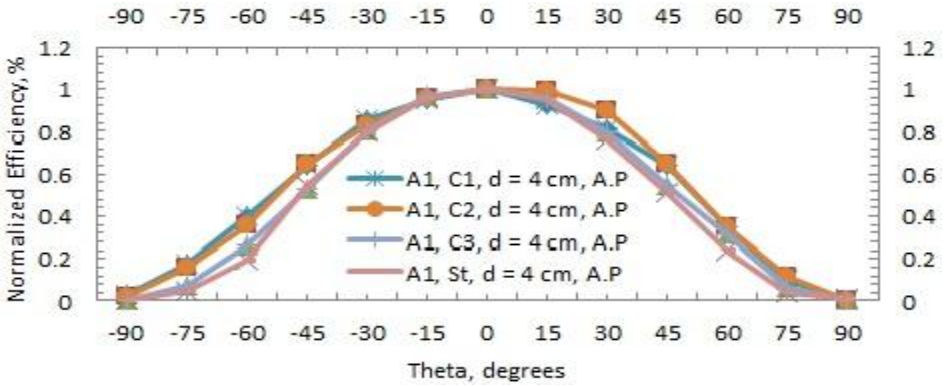


Figure 4.21 Antenna pattern curvature comparison for A1 at 4 cm distance

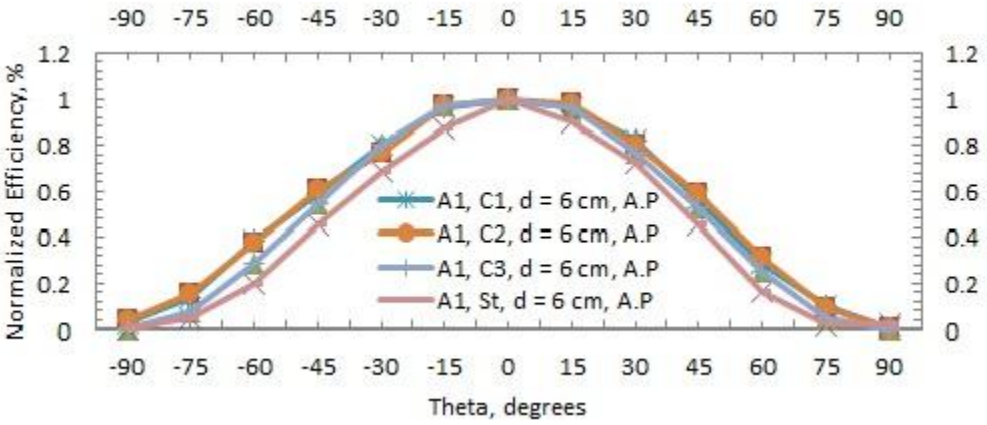


Figure 4.22 Antenna pattern curvature comparison for A1 at 6 cm distance

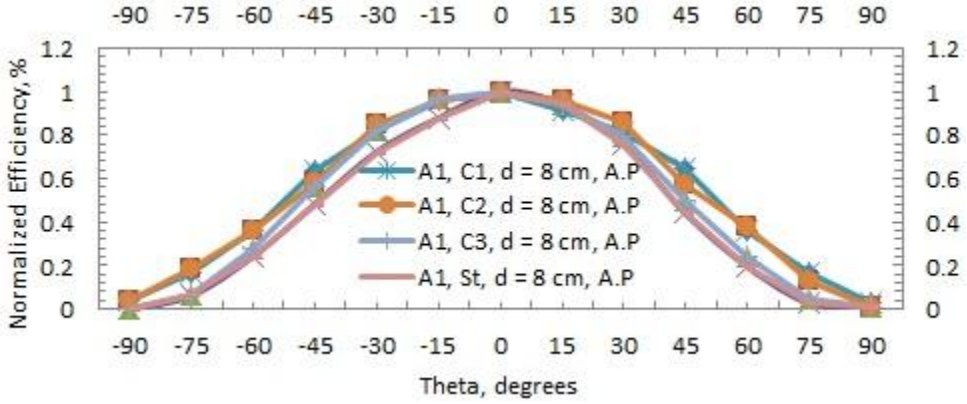


Figure 4.23 Antenna pattern curvature comparison for A1 at 8 cm distance

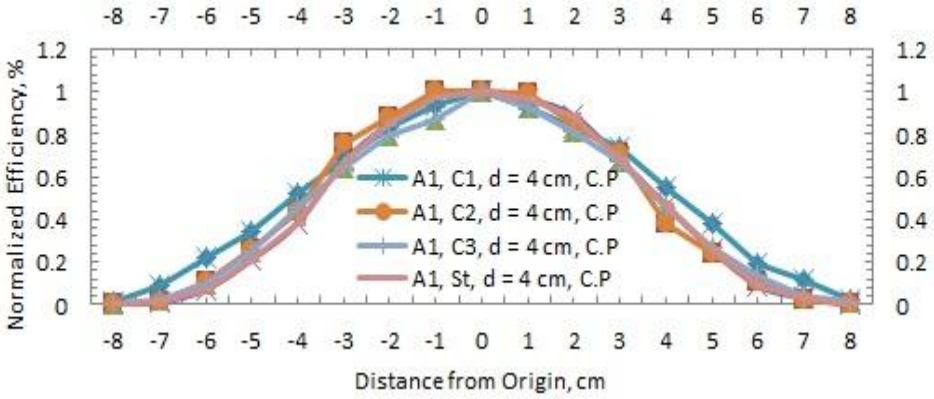


Figure 4.24 Cross-section pattern curvature comparison for A1 at 4 cm distance

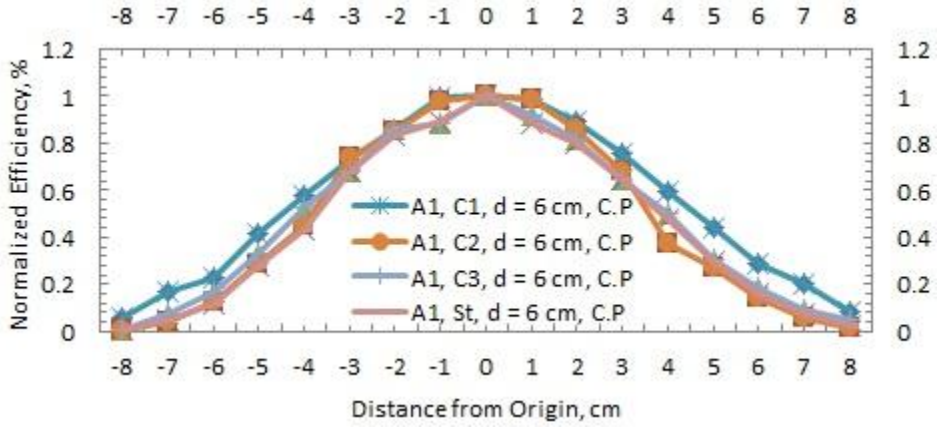


Figure 4.25 Cross-section pattern curvature comparison for A1 at 6 cm distance

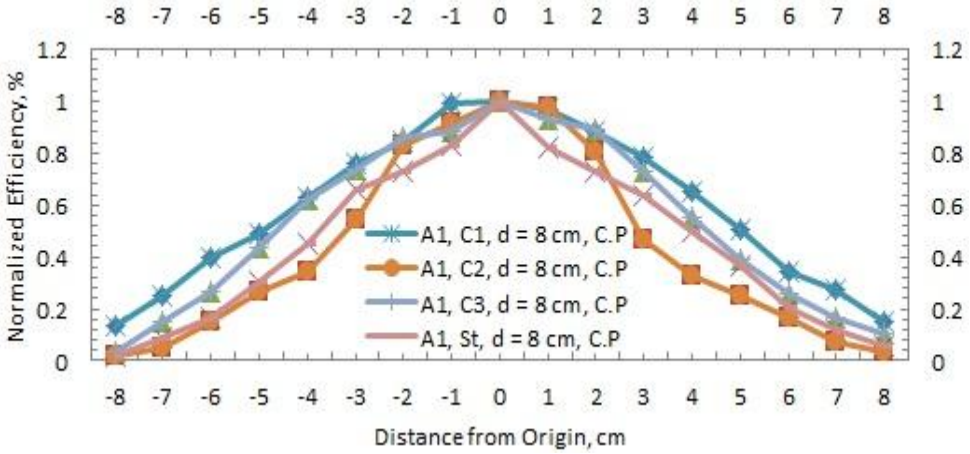


Figure 4.26 Cross-section pattern curvature comparison for A1 at 8 cm distance

From the curvature comparison results shown in Figure 4.18 – Figure 4.26, it is observed that the bandwidth increases with increase in bend and increase in distance. 3D plotting experiments were conducted later to obtain a plot at distances of 4 cm, 6 cm and 8 cm. 169 data points were collected at each distance.

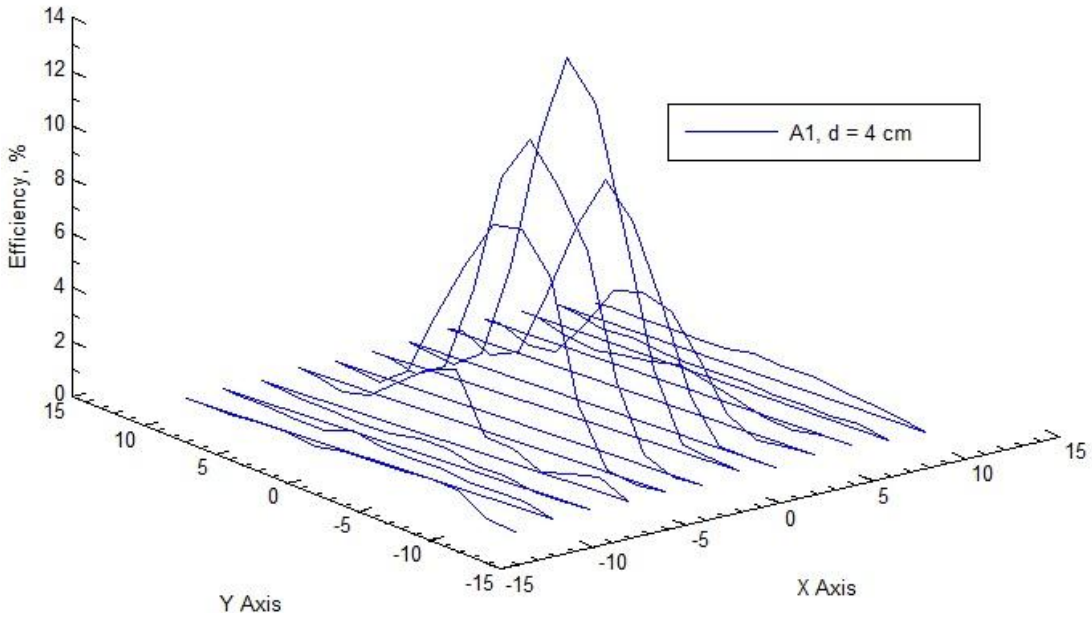


Figure 4.27 3D pattern for A1 at 4 cm distance

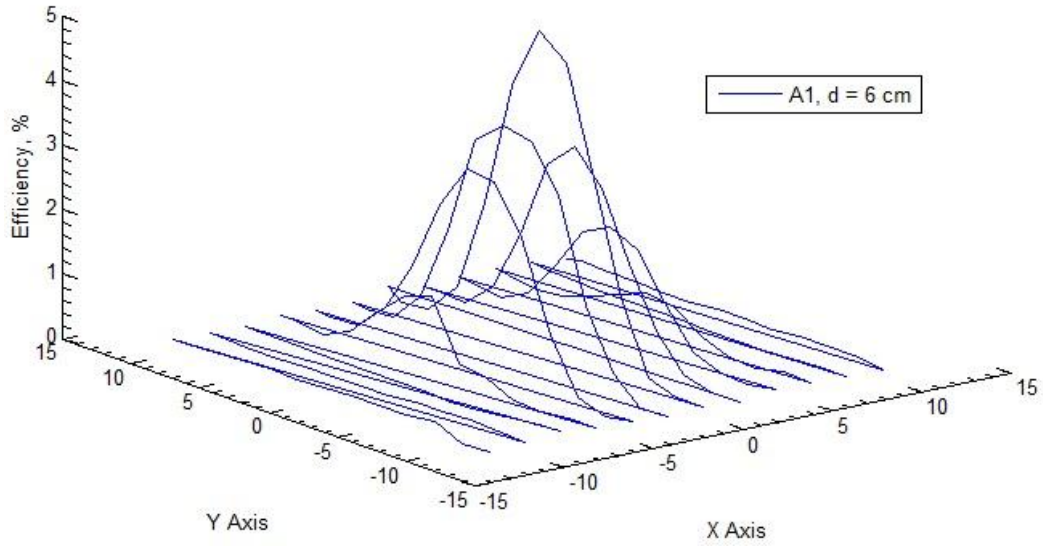


Figure 4.28 3D pattern for A1 at 6 cm distance

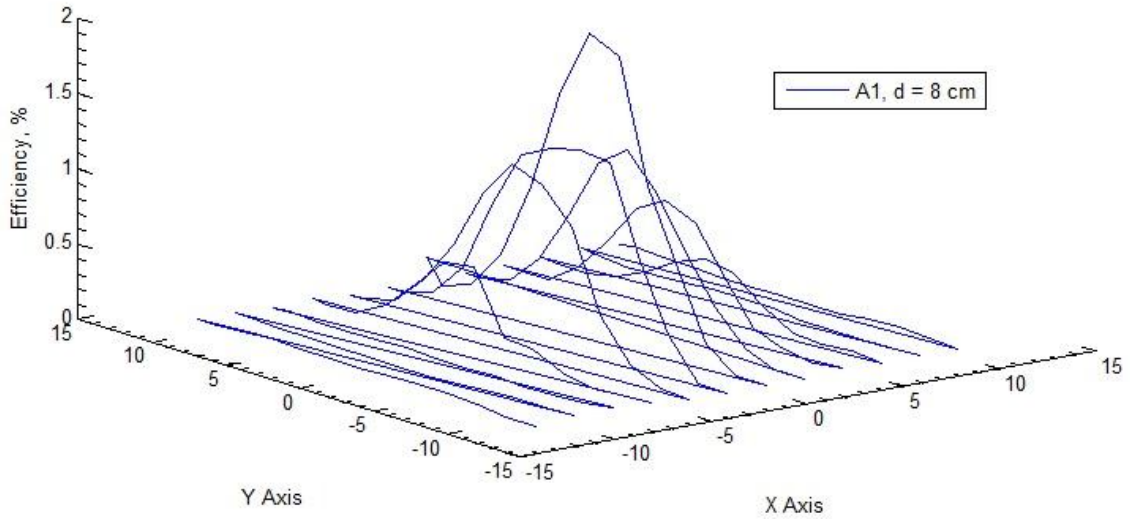


Figure 4.29 3D pattern for A1 at 8 cm distance

The above graphs show that a gaussian shaped curve is obtained at the efficiency measurements for each column. The gaussian shaped curve for the central column has the highest magnitude efficiency values. And the magnitude of the Gaussian curve decreases on either side of the central column.

In order to ascertain that all the graphs obtained for antenna A1 can be repeated for another flexible antenna design, a new antenna A2 with a different design mentioned in Table 4.1 was fabricated. The same number and type of experiments were conducted using A2. The results are shown in Figure 4.30 – Figure 4.52.

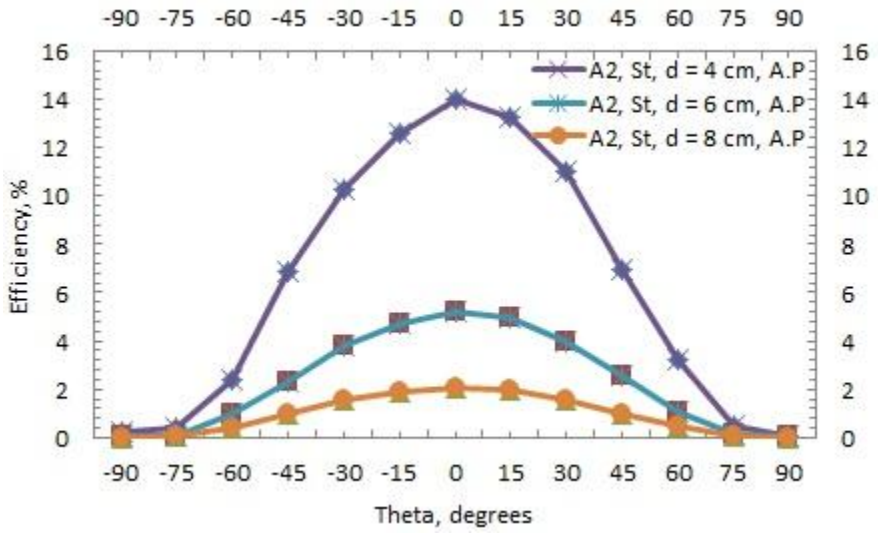


Figure 4.30 Antenna pattern distance comparison for A2 with flat bend

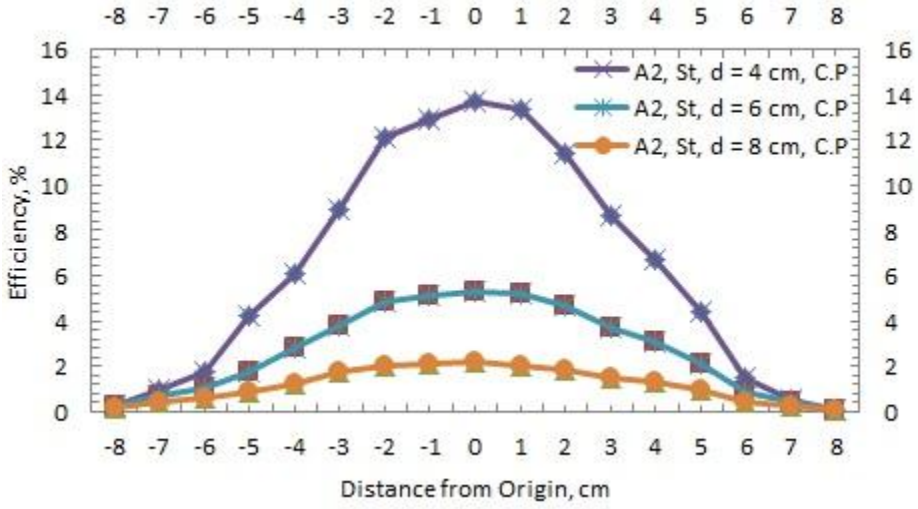


Figure 4.31 Cross-section pattern distance comparison for A2 with flat bend

The maximum efficiency obtained using the straight reader antenna is around 13 % – 14 % when the two coils are center aligned. From the comparison graphs, it is observed that the efficiency reduces with distance. The efficiency pattern has a gaussian shape for misalignment pattern, antenna pattern and cross section pattern experiments. The graphical results for the least bend curvature i.e. C3 are shown in Figure 4.32 – Figure 4.34.

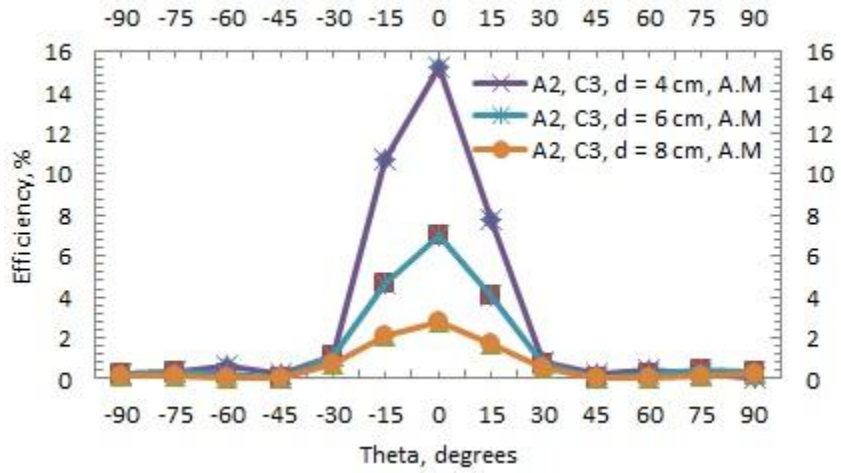


Figure 4.32 Antenna misalignment distance comparison for A2 with C3 bend

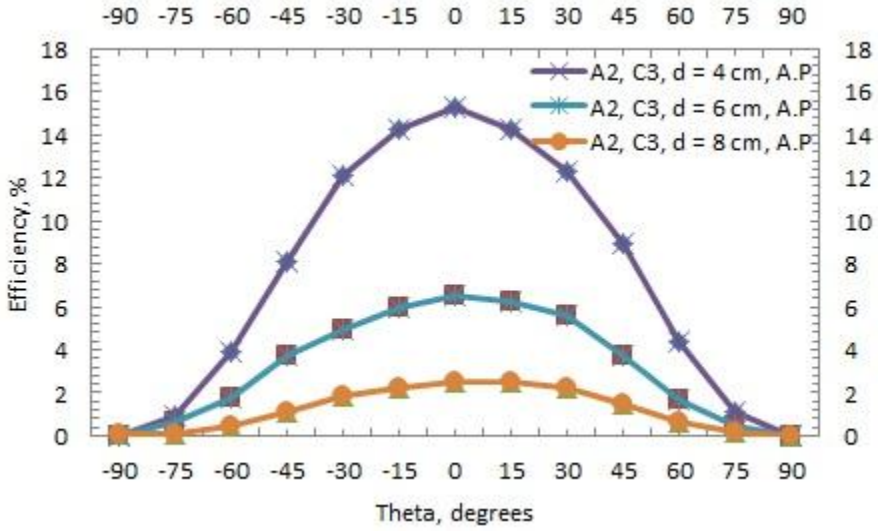


Figure 4.33 Antenna pattern distance comparison for A2 with C3 bend

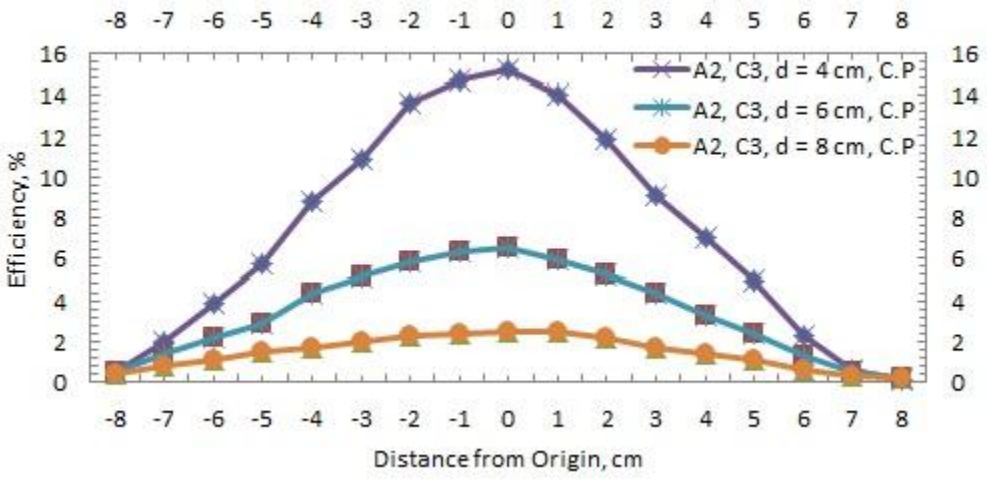


Figure 4.34 Cross-section pattern distance comparison for A2 with C3 bend

The maximum efficiency obtained with the reader antenna bent at C3 with the two coils center aligned increases to around 15 %. From the comparison graphs, it is observed that the efficiency reduces with distance. The efficiency pattern has a gaussian shape for misalignment pattern, antenna pattern and cross section pattern experiments. The graphical results for C2 bend is shown in Figure 4.35 – Figure 4.37.

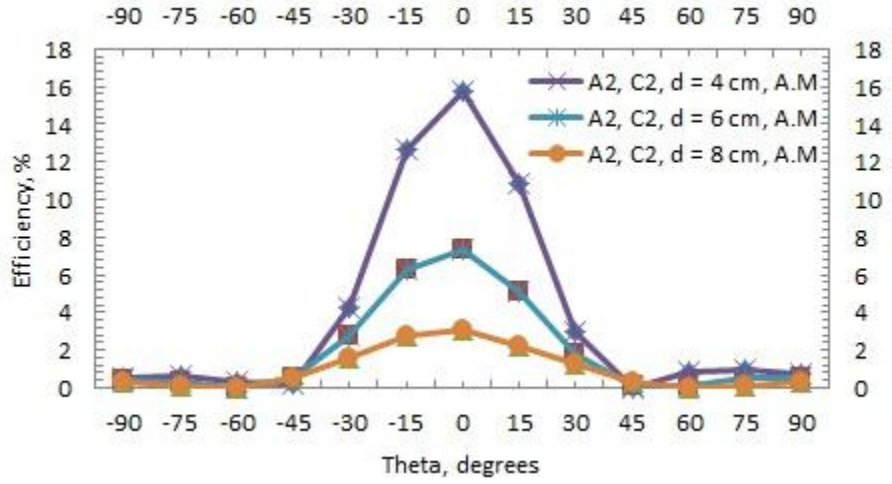


Figure 4.35 Antenna misalignment distance comparison for A2 with C2 bend

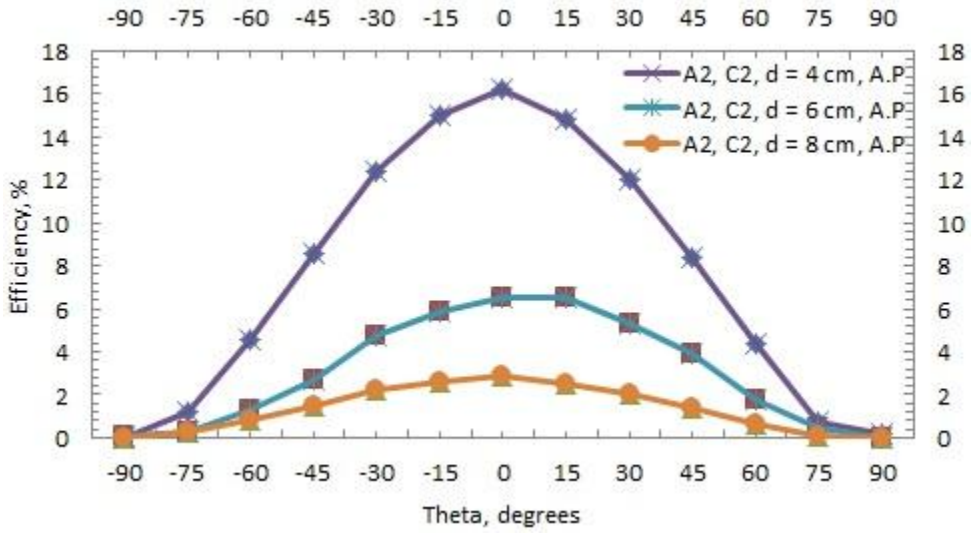


Figure 4.36 Antenna pattern distance comparison for A2 with C2 bend

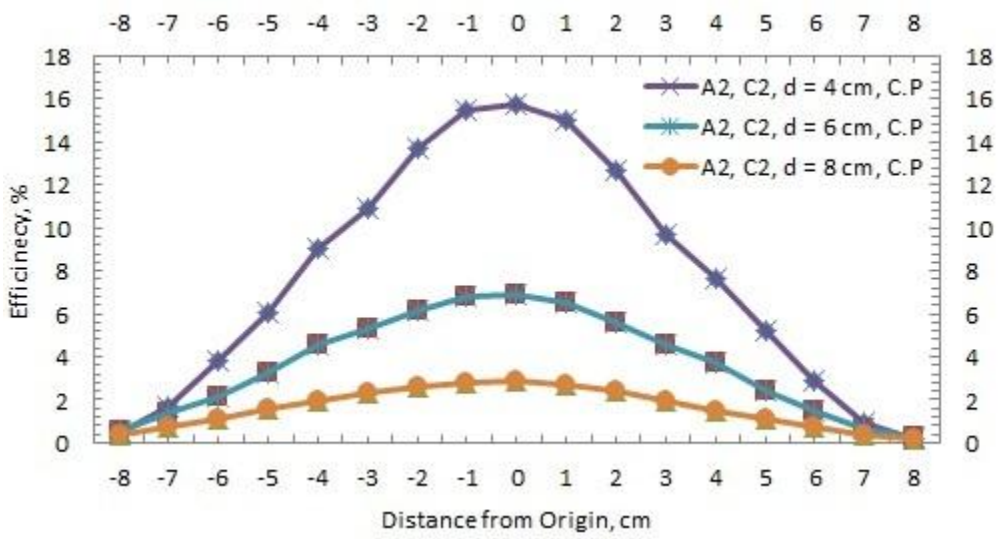


Figure 4.37 Cross-section pattern distance comparison for A2 with C2 bend

The maximum efficiency obtained with the reader antenna bent at C2 with the two coils center aligned increases to around 16 % - 17 %. From the comparison graphs, it is observed that the efficiency reduces with distance. The efficiency pattern has a gaussian shape for misalignment pattern, antenna pattern and cross section pattern experiments. The graphical results for C1 bend is shown in Figure 4.38 – Figure 4.40.

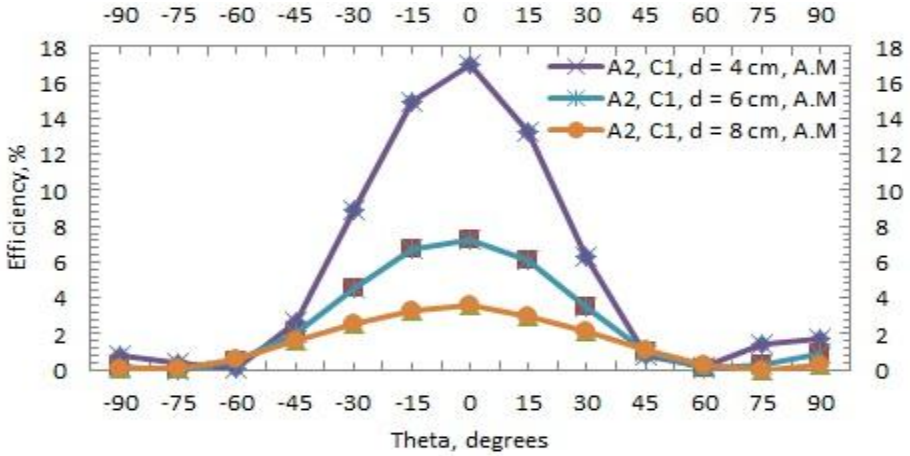


Figure 4.38 Antenna misalignment distance comparison for A2 with C1 bend

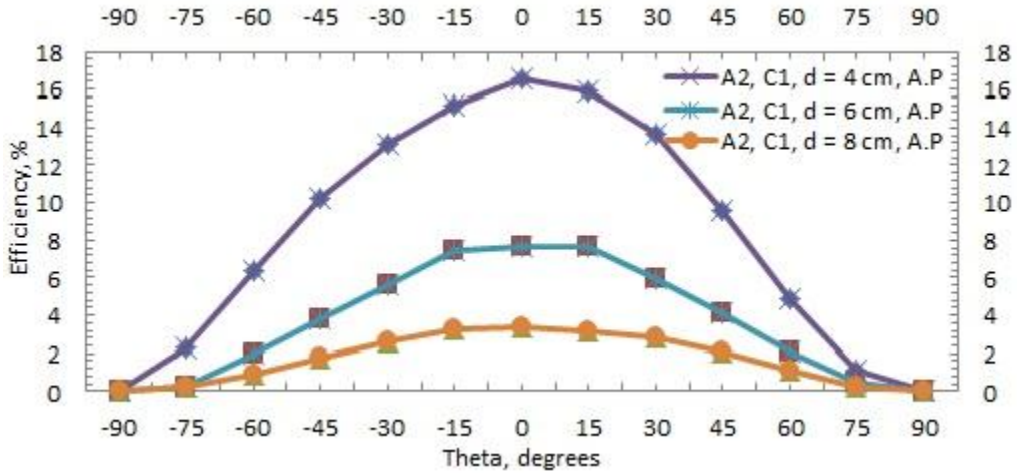


Figure 4.39 Antenna pattern distance comparison for A2 with C1 bend

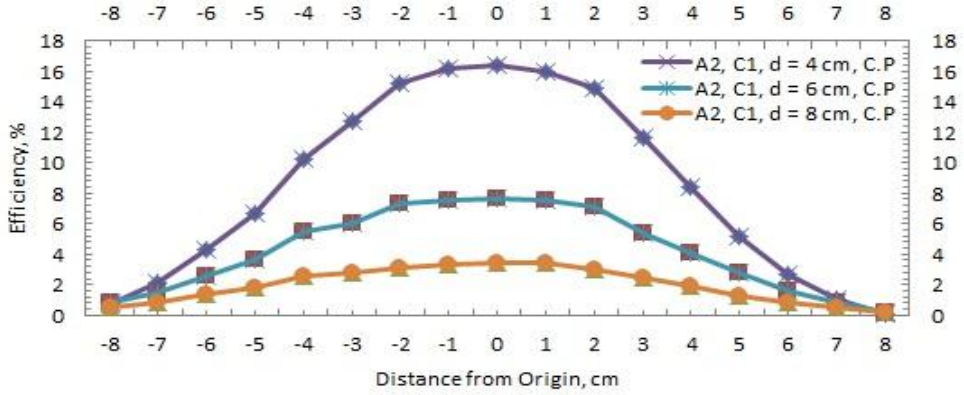


Figure 4.40 Cross-section pattern distance comparison for A2 with C1 bend

The maximum efficiency obtained with the reader antenna bent at C1 with the two coils center aligned increases to around 18%. From the comparison graphs, it is observed that the efficiency reduces with distance which can be explained from inverse square law. The efficiency pattern has a gaussian shape for misalignment pattern, antenna pattern and cross section pattern experiments. Graphs of different curvatures are then compared keeping the parameter, distance as constant.

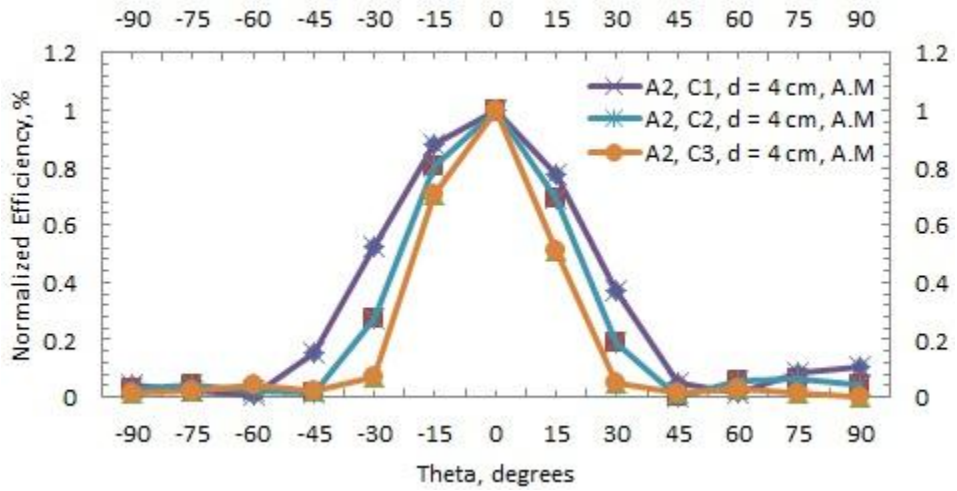


Figure 4.41 Antenna misalignment curvature comparison for A2 at 4 cm distance

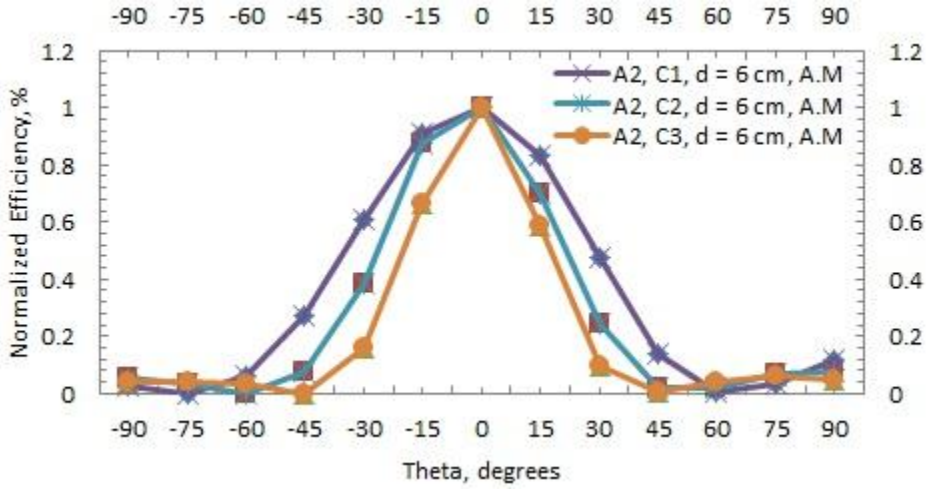


Figure 4.42 Antenna misalignment curvature comparison for A2 at 6 cm distance

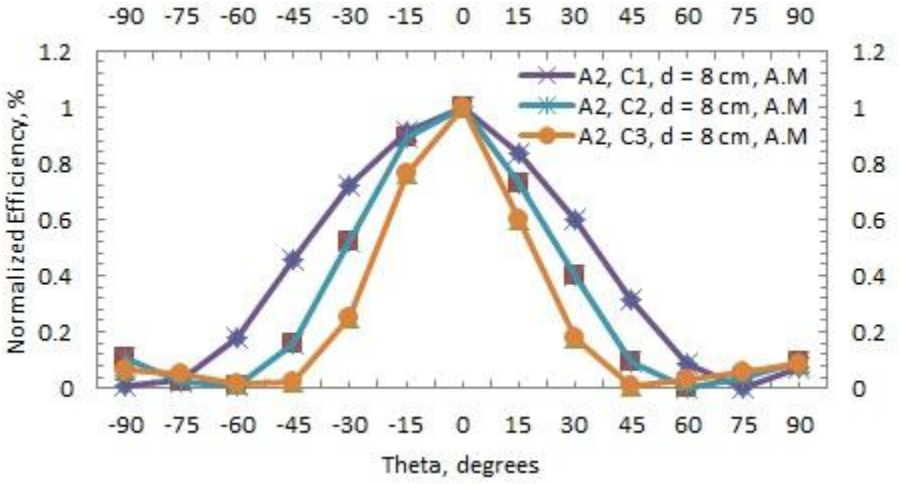


Figure 4.43 Antenna misalignment curvature comparison for A2 at 8 cm distance

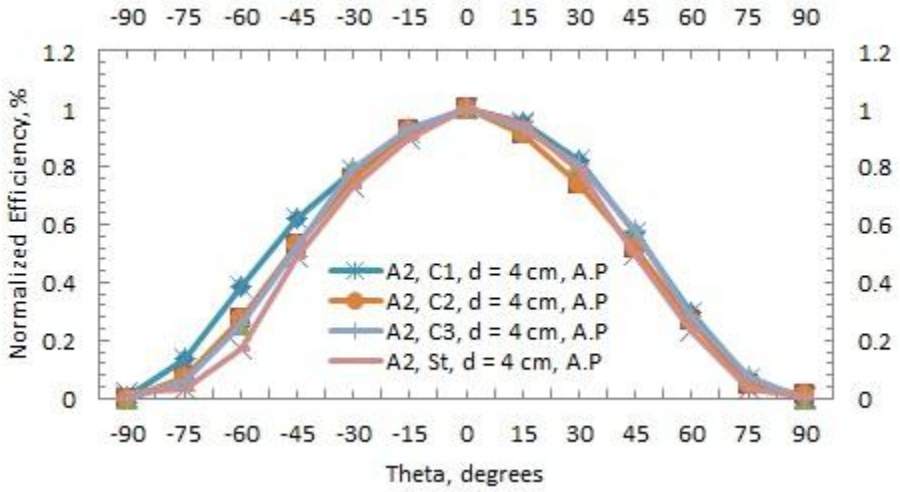


Figure 4.44 Antenna pattern curvature comparison for A2 at 4 cm distance

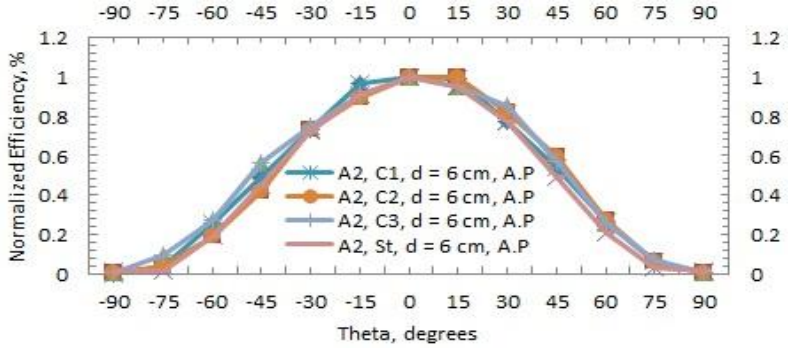


Figure 4.45 Antenna pattern curvature comparison for A2 at 6 cm distance

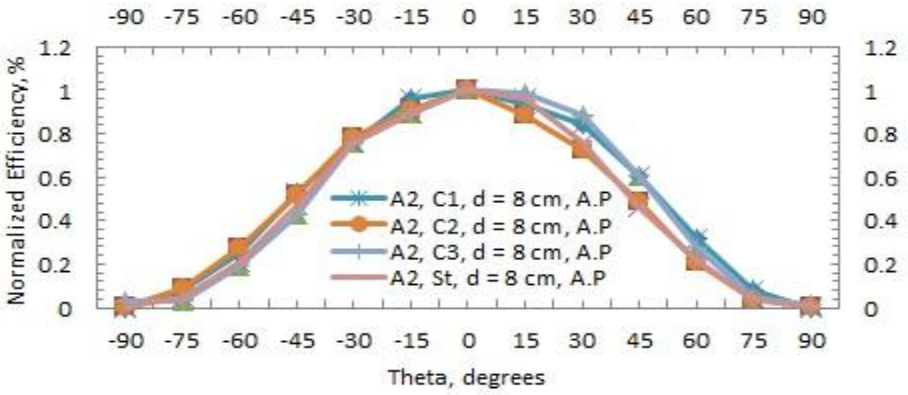


Figure 4.46 Antenna pattern curvature comparison for A2 at 8 cm distance

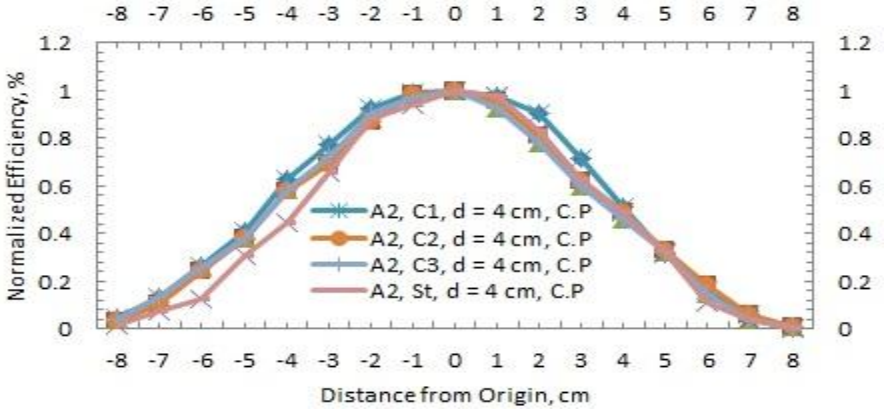


Figure 4.47 Cross-section pattern curvature comparison for A2 at 4 cm distance

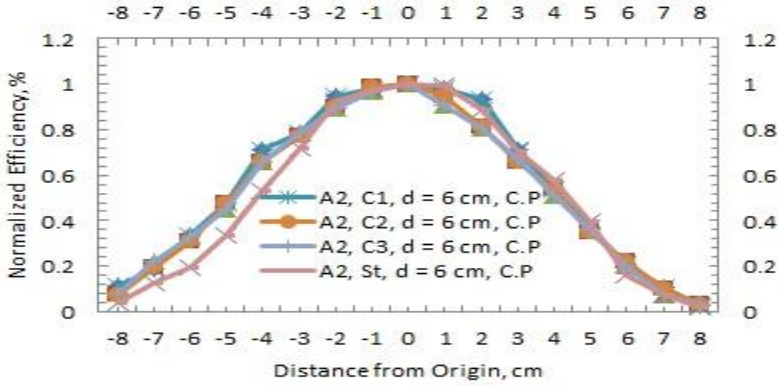


Figure 4.48 Cross-section pattern curvature comparison for A2 at 6 cm distance

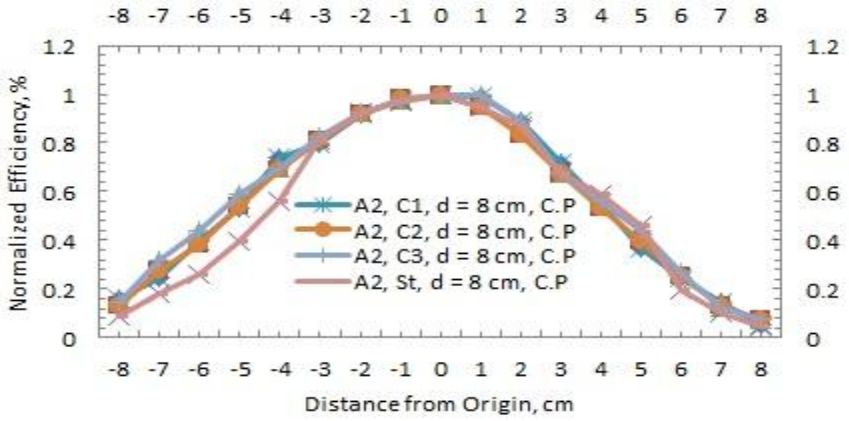


Figure 4.49 Cross-section pattern curvature comparison for A2 at 8 cm distance

From the curvature comparison results shown in Figure 4.41 – Figure 4.49, it is observed that the bandwidth increases with increase in bend and increase in distance. 3D plotting experiments were conducted later to obtain a plot at distances of 4 cm, 6 cm and 8 cm. 169 data points were collected at each distance.

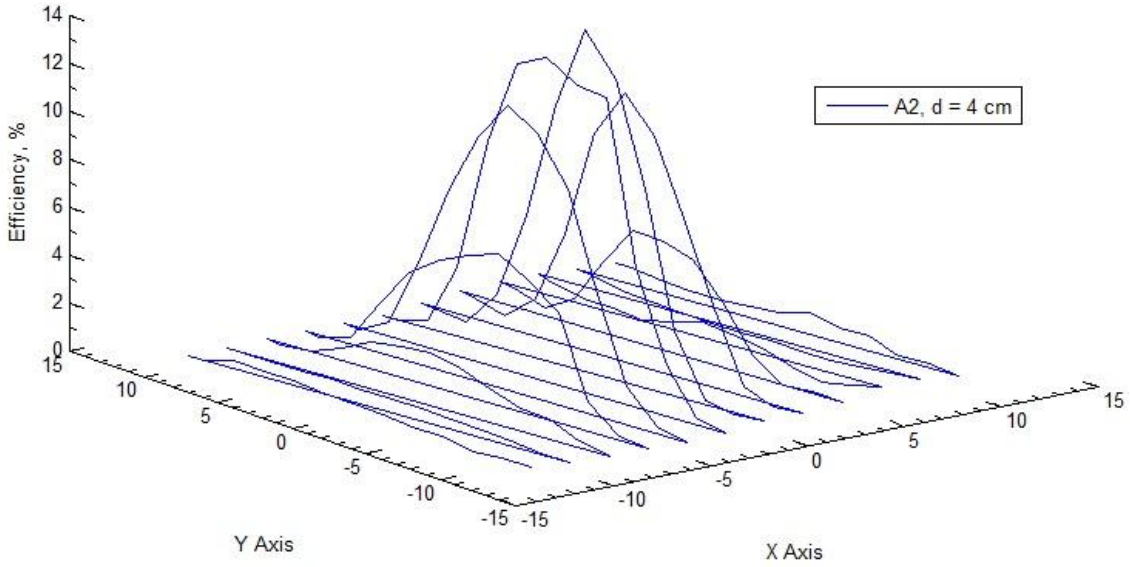


Figure 4.50 3D pattern for A2 at 4 cm distance

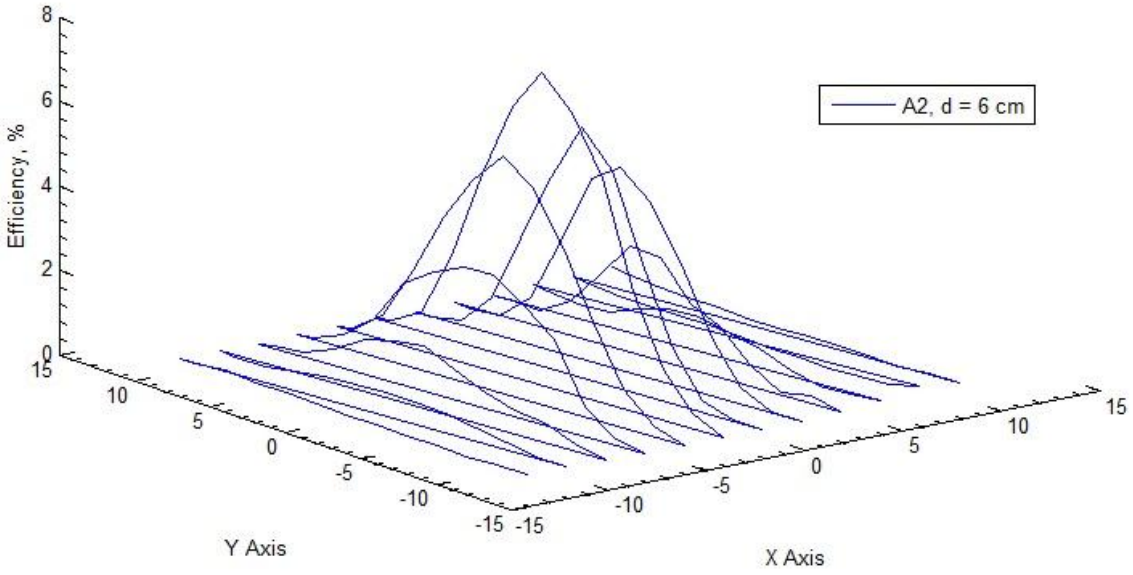


Figure 4.51 3D pattern for A2 at 6 cm distance

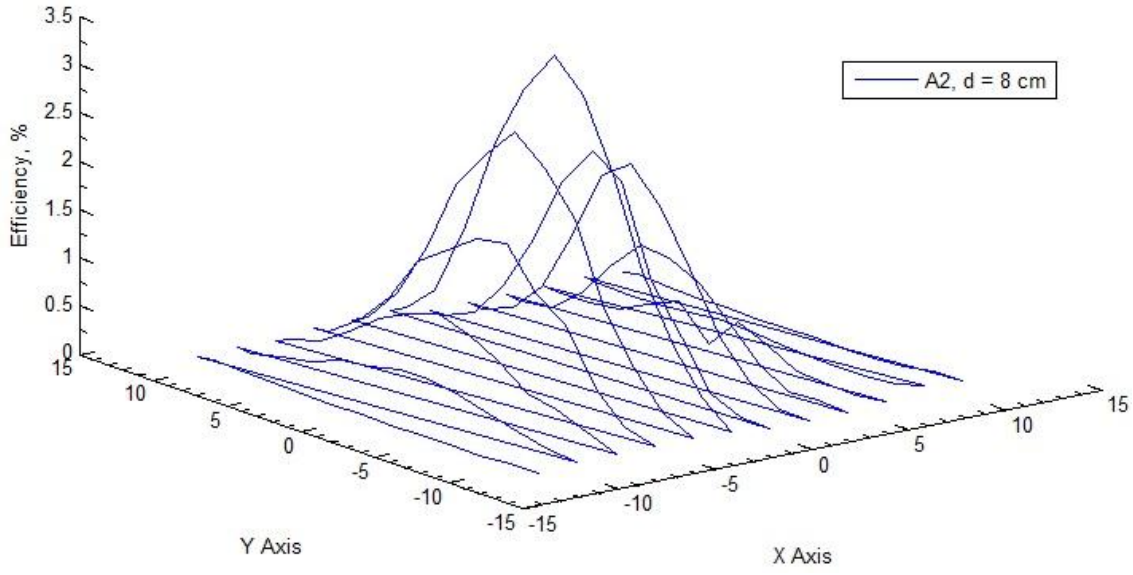


Figure 4.52 3D pattern for A2 at 8 cm distance

The above graphs show that a Gaussian curve is obtained at the efficiency measurements for each column. The Gaussian curve for the central column has the highest magnitude efficiency values. And the magnitude of the Gaussian curve decreases on either side of the central column.

## 4.7 Explanation of the results

Faraday, showed that the magnitude of electromagnetic force generated in the coil is proportional to the rate of change of magnetic flux passing through all the turns of the coil. With the displacement of either antenna that causes misalignment between the centers of the two coils, the passage of magnetic flux through all the turns of the Tag antenna reduces, thus causing the reduction in emf generated at the tag coil, hence the reduction in efficiency. This phenomenon is verified by the graphs obtained.

It was found from experiments that by using a straight coil, the efficiency obtained is around 12% which is less than other curvatures used. By increasing the distance between reader antenna and the tag antenna the efficiency decreases, because of the inverse square law. From the graphs, it is observed that the efficiency of power transfer decreases on either side of the zero position of the reader antenna. The curve is Gaussian shaped, and since the power transferred between the two antennas is due to change in magnetic flux linking the two coils, the intensity of magnetic field distribution on either side of the zero position is gaussian. Gaussian distribution of magnetic field intensity is observed, when both the reader and tag coils are rotated, keeping either antenna static when the other is rotated. Also the cross section pattern follows a gaussian distribution, indicating that the magnetic flux density is strongest at the center of the antenna and reduces in a gaussian manner, as the tag antenna is moved away from the center. From, the comparison graphs shown above, a summarized picture of the magnetic field distribution is obtained. The 3D pattern gives a better picture of the magnetic field distribution between the reader and tag antennas. From the gaussian shaped curves obtained by moving the tag across each row of the tag plate, it is understood how the magnetic field

varies in the three dimensional region between the reader antenna and tag antenna. The gaussian shape of the curves can be explained by the below formulas [31].

$$W(\theta,\phi) = \frac{G(\theta,\phi)}{4\pi r^2} P_t \tag{4.4}$$

where *W* is the power density of the incident radiation from the reader antenna. $\theta$ and $\phi$ indicate the direction dependence of the parameters. *G* is the gain of the reader antenna which is dependent on the radiation efficiency, antenna gain and mismatch losses between reader antenna and transmitter circuit. $P_t$ is the power the reader antenna would deliver to a matched load. *r* is the distance between the reader and tag antennas.

$$P_r = A(\theta,\phi)W \tag{4.5}$$

where $P_r$ is the power delivered to the tag antenna, A is the effective aperture of the tag antenna which is the effective area of the tag antenna that directly intercepts the power transmitted by the reader antenna.

$$\frac{P_r}{P_t} = A\frac{G}{4\pi r^2} \tag{4.6}$$

(4.6) is obtained from (4.4) and (4.5) and is the efficiency of power received at the tag antenna. The efficiency depends on the effective aperture of tag antenna, gain of the reader antenna and the distance between the tag and reader antennas. The gain of the reader antenna is constant since the source is constant. Hence the curves obtained in Figure 4.7 – Figure 4.52 are dependent on the effective aperture of the tag antenna and the distance between the tag and reader antennas.

By increasing the bend of the coil by using pvc pipes, an efficiency of around 14%, 16% and 18% is obtained between center-aligned reader and tag antennas. Thus there is approximately, an increase of 2% in the power transfer efficiency with the increase in the bending radius of the coil by 4 cm. This hints that the magnetic flux at the center of the two coils

increases due to contribution from the sides of the reader antenna. And with the increase in bend, the contribution made from either side of the reader antenna center, increases.

# CHAPTER 5

# CONCLUSION

Simulation model was established using Ansoft HFSS program. To ensure simulation results obtained from Ansoft HFSS software are accurate a spiral antenna simulation model had to be established. Planar spiral antenna formulae referred from [17] were used. Since the results obtained from these formulae are only valid at dc frequencies, different spiral antenna designs were used and simulated to match the results obtained from the formulae. The results matched. Two IEEE papers [16, 24] were used to ascertain whether the model is correct. Inductance and quality factor results obtained from these two papers also matched with the appropriate models made in HFSS.

The experimental results validated simulation model. The next step was to ascertain whether the experimentally fabricated inductor results matched the HFSS simulation results. Two different substrates, wood and kapton, were used and 35 experiments were conducted using inductors of different design. The simulation results matched the HFSS model in all the experiments.

Power transfer efficiency and radiation pattern were experimentally tested. A total of 125 experiments were conducted using a stable well designed setup. Experiments were conducted using two different reader antennae, three different bending angles of reader antenna at three different distances. All results obtained were compared with results obtained from a straight reader antenna. 3D radiation pattern experiments were conducted and the results obtained, establish the radiation pattern in the space between the reader and tag antenna. Using four different experiments the power transfer efficiency was obtained and the radiation pattern was thus established.

Flat and curve antenna with three different curvatures were tested. Three different curvatures C1 of 8.4 cm bend, C2 of 11.4 cm bend and C3 of 14 cm bend were used in the characterization experiments and the reader antenna was bent along these curvatures and tested. The antenna pattern comparison results show that the pattern does not change with bending. Also the efficiency increases with increase in bend.

The antenna misalignment experiment suggests that when the patient wears the reader antenna in the wrong position the radiation pattern changes for different degree of reader antenna bend. The antenna pattern experiment suggests that when the tag antenna inside the body moves along its axis the radiation pattern does not change for different degree of reader antenna bend. The cross-section pattern experiment suggests that when the doctor commits a mistake in aligning the tag antenna with the reader antenna while inserting the implant inside the patient using endoscopy, the radiation pattern does not change for different degree of reader antenna bend. The 3D radiation pattern experiment indicates the working zone of the tag antenna when it is attached to a sensor. From these experiments, it can be concluded that the radiation pattern will change if the reader antenna moves but the pattern will not change if the tag antenna moves for different degree of reader antenna bend. These results prove that flexible antennas can be used for wireless powering of medical implants since bending the antenna only improves the efficiency and does not change the antenna pattern.

CHAPTER 6

FUTURE WORK

## 6.1 Agilent module

In the thesis work discussed, all characterization results were obtained manually. This involved weeks of work in collecting and processing data, the time spent in fabricating the setup etc. A major chunk of the time was consumed in ensuring that the reader and tag antennas are perfectly aligned at the respective orientations. This involved repetition of the results to ensure stable graphical results. Several companies have built different types of modules involving high – tech gadgets for accurately obtaining thousands of data points in a short period of time. One such gadget is the one built by Agilent [12]. A pictorial diagram of the module is shown in Figure 6.1.

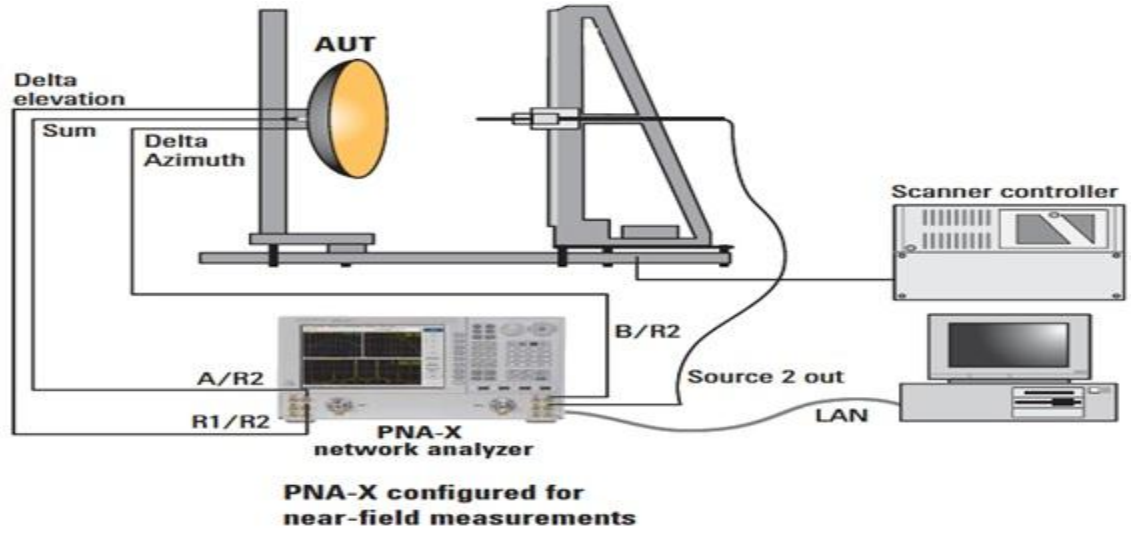


Figure6.1 Agilent module[12]

From the module shown, the bending angle of the flexible antenna can be controlled. The power pattern can be obtained in the 3 dimensional space surrounding the antenna by using a scanner controller device. The PNA – X network analyzer can be configured for both near-field and far-

field measurements. The data collected by the network analyzer can then be stored in a computer.

More than forty thousand data points can be obtained in a time interval of 10 to 20 minutes, thus reducing the experimental time by one tenths. Also there is no human intervention, since the experiments conducted are controlled automatically, thus improving the reliability of the results obtained. Optimum Measurement sensitivity is a critical aspect for antenna measurements, which is provided by the device.

In the future, reliable characterization experiments can be conducted using this module for any kind of antenna in a short interval of time.

## 6.2 Stacked spiral antennas

By making use of flexible stacked antennas, the inductive power transfer can be increased and the resonant magnetic coupling frequency can be reduced [10, 30], thereby reducing the power absorbed by the body tissues and increasing the range of operation. Characterization of these antennas is therefore important.

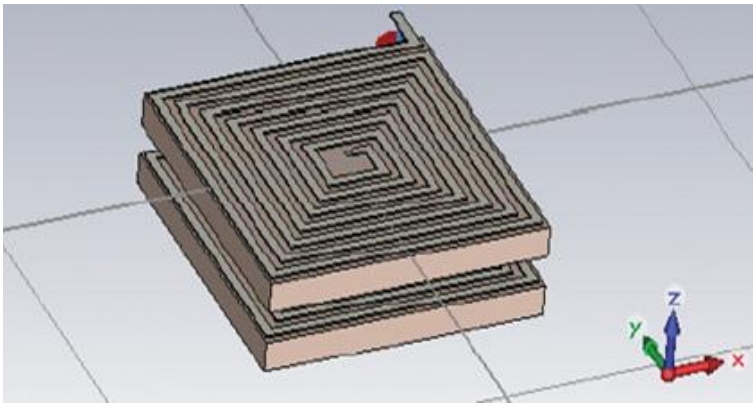


Figure 6.2 Stacked spiral antenna [10]

# APPENDIX A

## MATERIAL DATA SHEETS AND SPECIFICATIONS

## A.1 KAPTON DATA SHEET

Kapton is a biocompatible material used as a substrate for fabrication of flexible antennas. Their characteristics are discussed in Table 1, Table 2 and Table 3.

TABLE 1
Typical Electrical Properties of DuPont™ Kapton® HN Film at 23°C (73°F), 50% RH

| Property<br>Film Gage | Typical Value | Test Condition | Test Method |
|---|---|---|---|
| Dielectric Strength<br>25 µm (1 mil)<br>50 µm (2 mil)<br>75 µm (3 mil)<br>125 µm (5 mil) | V/m kV/mm (V/mil)<br>303 (7700)<br>240 (6100)<br>205 (5200)<br>154 (3900) | 60 Hz<br>1/4 in electrodes<br>500 V/sec rise | ASTM D-149-91 |
| Dielectric Constant<br>25 µm (1 mil)<br>50 µm (2 mil)<br>75 µm (3 mil)<br>125 µm (5 mil) | <br>3.4<br>3.4<br>3.5<br>3.5 | 1 kHz | ASTM D-150-92 |
| Dissipation Factor<br>25 µm (1 mil)<br>50 µm (2 mil)<br>75 µm (3 mil)<br>125 µm (5 mil) | <br>0.0018<br>0.0020<br>0.0020<br>0.0026 | 1 kHz | ASTM D-150-92 |
| Volume Resistivity<br>25 µm (1 mil)<br>50 µm (2 mil)<br>75 µm (3 mil)<br>125 µm (5 mil) | •cm<br>$1.5 \times 10^{17}$<br>$1.5 \times 10^{17}$<br>$1.4 \times 10^{17}$<br>$1.0 \times 10^{17}$ | | ASTM D-257-91 |

TABLE 2
Thermal Properties of DuPont™ Kapton® HN Film

| Thermal Property | Typical Value | Test Condition | Test Method |
|---|---|---|---|
| Melting Point | None | None | ASTM E-794-85 (1989) |
| Thermal Coefficient of Linear Expansion | 20 ppm/°C<br>(11 ppm/°F) | -14 to 38°C<br>(7 to 100°F) | ASTM D-696-91 |
| Coefficient of Thermal Conductivity,<br>W/m•K<br>cal / cm•sec•°C | 0.12<br>$2.87 \times 10^{4}$ | 296K<br>23°C | ASTM F-433-77 (1987) |
| Specific Heat, J/g•K (cal/g•°C) | 1.09 (0.261) | | Differential calorimetry |
| Heat Sealability | not heat sealable | | |
| Solder Float | pass | | IPC-TM-650<br>Method 2.4.13A |
| Smoke Generation | $D_m$=<1 | NBS<br>smoke chamber | NFPA-258 |
| Shrinkage, %<br>30 min at 150°C<br>120 min at 400°C | <br>0.17<br>1.25 | | IPC-TM-650<br>Method 2.2.4A;<br>ASTM D-5214-91 |
| Limiting Oxygen Index, % | 37–45 | | ASTM D-2863-87 |
| Glass Transition Temperature ($T_g$) | A second order transition occurs in Kapton® between 360°C (680°F) and 410°C (770°F) and is assumed to be the glass transition temperature. Different measurement techniques produce different results within the above temperature range. | | |

TABLE 3

Physical Properties of DuPont™ Kapton® HN at 23°C (73°F)

| Property | Unit | 1 mil 25µm | 2 mil 50µm | 3 mil 75µm | 5 mil 125µm | Test Method |
|---|---|---|---|---|---|---|
| Ultimate Tensile Strength<br>at 23°C, (73°F)<br>at 200°C (392°F) | psi (MPa) | 33,500(231)<br>20,000(139) | 33,500(231)<br>20,000(139) | 33,500(231)<br>20,000(139) | 33,500(231)<br>20,000(139) | ASTM D-882-91, Method A* |
| Ultimate Elongation<br>at 23°C, (73°F)<br>at 200°C (392°F) | % | 72<br>83 | 82<br>83 | 82<br>83 | 82<br>83 | ASTM D-882-91, Method A |
| Tensile Modulus<br>at 23°C, (73°F)<br>at 200°C (392°F) | psi (GPa) | 370,000 (2.5)<br>290,000 (2.0) | 370,000 (2.5)<br>290,000 (2.0) | 370,000 (2.5)<br>290,000 (2.0) | 370,000 (2.5)<br>290,000 (2.0) | ASTM D-882-91, Method A |
| Density | g/cc | 1.42 | 1.42 | 1.42 | 1.42 | ASTM D-1505-90 |
| MIT Folding Endurance | cycles | 285,000 | 55,000 | 6000 | 5,000 | ASTM D-2176-89 |
| Tear Strength-propagating (Elmendorf), N (lbf) | | 0.07<br>(0.02) | 0.21<br>(0.02) | 0.38<br>(0.02) | 0.58<br>(0.02) | ASTM D-1922-89 |
| Tear Strength, Initial (Graves), N (lbf) | | 7.2<br>(1.6) | 16.3<br>(1.6) | 26.3<br>(1.6) | 46.9<br>(1.6) | ASTM D-1004-90 |
| Yield Point at 3%<br>at 23°C, (73°F)<br>at 200°C (392°F) | MPa (psi) | 69 (10,000)<br>41 (6000) | 69 (10,000)<br>41 (6000) | 69 (10,000)<br>41 (6000) | 69 (10,000)<br>41 (6000) | ASTM D-882-91 |
| Stress to produce 5% elong.<br>at 23°C, (73°F)<br>at 200°C (392°F) | MPa (psi) | 90 (13,000)<br>61 (9000) | 90 (13,000)<br>61 (9000) | 90 (13,000)<br>61 (9000) | 90 (13,000)<br>61 (9000) | ASTM D-882-92 |
| Impact Strength<br>at 23°C, (73°F) | N•cm•(ft lb) | 78 (0.58) | 78 (0.58) | 78 (0.58) | 78 (0.58) | DuPont Pneumatic Impact Test |
| Coefficient of Friction, kinetic (film-to-film) | | 0.48 | 0.48 | 0.48 | 0.48 | ASTM D-1894-90 |
| Coefficient of Friction, static (film-to-film) | | 0.63 | 0.63 | 0.63 | 0.63 | ASTM D-1894-90 |
| Refractive Index (sodium D line) | | 1.70 | 1.70 | 1.70 | 1.70 | ASTM D-542-90 |
| Poisson's Ratio | | 0.34 | 0.34 | 0.34 | 0.34 | Avg. three samples, Elongated at 5, 7, 10% |
| Low temperature flex life | | pass | pass | pass | pass | IPC-TM-650, Method 2.6.18 |

## A2. JVCC CFL-5CA COPPER FOIL TAPE (CONDUCTIVE ADHESIVE) SPECIFICATIONS

- Adhesive: The bottom side of copper foil has conductive acrylic with the help of which it can stick on any material
- Carrier/Backing: copper foil
- Release Liner: 60# paper
- Thickness of tape: 3 mils (without liner) 1.6 mils (adhesive) 1.4 mils (carrier/backing)
- Adhesion: 70 ounces per inch (to stainless steel)
- Tensile Strength: 36 pounds per inch (longitudinal)
- Service/Operating Temperature: up to 311°F
- Elongation: 6%
- Electrical Resistance: 0.003 Ohms/sq. in.
- Certifications: File #130121, UL510, Section 4, MIL-T-47012
- Core: 3" diameter neutral

# APPENDIX B

# MATLAB PROGRAMS

## B1. CURRENTSHEET AND WHEELER FORMULAE

Matlab [14] codes were written for speedy calculation of inductances using formulas mentioned in [17].

Currentsheet Function

```
function [Lgmd]=currentsheet(n,din,dout)
mu = 4*3.141592654*(10^-7);
c1 = 1.27;
c2 = 2.07;
c3 = 0.18;
c4 = 0.13;
davg = (dout+din)*0.5*(10^-3);
p = (dout - din)/(dout + din);
Lgmd = ((0.5*mu*(n^2)*davg*c1)*(loge(c2/p)+(c3*p)+(c4*(p^2))))*(10^6);
End
```

Wheeler Function

```
function [Lmw]=wheeler(n,din,dout)
k1 = 2.34;
k2 = 2.75;
davg = 0.5*(10^-3)*(dout+din);
p = (dout - din)/(dout + din);
Lmw = (k1*4*3.141592654*(10^-7)*(((n^2)*davg)/(1+(k2*p))))*(10^6);
End
```

## B2. 3D PATTERN MATLAB PROGRAM

Also a matlab code was written to plot the 3D pattern graphs. The value of X axis and Y axis was given as input. The value of Z axis which is the efficiency values at corresponding value of X and Y are also given as input. The 3D pattern graph was then obtained using the in-built matlab function -

plot3 (X,Y,Z)

legend ('Ax, d = x cm').

REFERENCES

[1] Upkar Varshney “Pervasive Healthcare and Wireless Health Monitoring”, Journal of Mobile Networks and Applications, Volume 12, Issue 2-3, March 2007, Pages 113 – 127.

[2] Xiaoyu Liu, Fei Zhang, Steven A. Hackworth, Robert J. Sclabassi and Mingui Sun “Wireless Power Transfer System Design for Implanted and Wom Devices”, Bioengineering Conference, 2009 IEEE 35th Annual North East.

[3] Anthony N. Laskovski, Tharaka Dissanayake and Mehmet R. Yuce “Wireless Power Technology for Biomedical Implants”, Biomedical Engineering, pp 119 – 132.

[4] James W. (“Rus”) Healy “Antenna Here is a Dipole”, NJ2L.

[5] Thermpon Ativanichayaphong “Wireless Devices for Medical Applications”, ProQuest, The University of Texas at Arlington, Electrical Engineering, December 2007.

[6] Anders J Johansson “Wireless Communication with Medical Implants : Antennas and Propagation”, Department of Electroscience, Lund University, June 2004.

[7] Jaime Garnica, Joaquin Casanova, and Jenshan Lin “High Efficiency Midrange Wireless Power Transfer System”, IMWS-IWPT2011 Proceedings.

[8] Teck Chuan Beh, Takehiro Imura, Masaki Kato, Yoichi Hori, “Wireless Power Transfer System via Magnetic Resonant Coupling at Restricted Frequency Range – Fixing Resonace Frequency With Impedance Matching”, University of Tokyo, 2010.

[9] Nathan O. Sokal “Class – E RF Power Amplifiers”, WA1HQC of Design Automation, Inc, Jan/Feb 2001.

[10] Anthony Nikola Laskovski, Mehmet Rasit Yuce, and Tharaka Dissanayake, “Stacked Spirals for Biosensor Telemetry”, IEEE Sensors Journal, VOL. 11, No. 6, June 2011.

[11] P. R. Troyk and G. A. DeMichele, “Inductively-coupled power and data link for neural prostheses using a class-E oscillator and FSK modulation,” IEEE International Conference Engineering in Medicine and Biology Society, Vol.4, pp.3376-3379, 2003.

[12] Agilent Technologies “Solutions for Antenna Characterization”

[13] Ansoft Corporation “Ansoft High Frequency Structure Simulator v10 User’s Guide”, 2005.

[14] Christos Xenophontos “A Beginner’s Guide to MATLAB”, Department of Mathematical Sciences, Loyola College.

[15] Oleksiy Klymenko “UWB Receiver Frontend Design with ADS”, ADS User Group Meeting, IHP, Frankfurt, Germany, pp 13 – 15, May 14 & 15, 2009.

[16] Uei – Ming Jow, Maysam Ghovanloo “Modeling and Optimization of Printed Spiral Coils in Air, Saline, and Muscle Tissue Environments”, IEEE Transactions on Biomedical Circuits and Systems, Vol . 3, No. 5, October 2009.

[17] Sunderajan S.Mohan, Maria del Mar Hershenson, Stephen P. Boyd, and Thomas H.Lee "Simple Accurate Expressions for Planar Spiral Inductances", IEEE Journal of Solid-State Circuits, Vol. 34, No. 10, October 1999.

[18] AutoDesk Official Training Guide “Autocad 2010 Volume 1”, April 2009.

[19] AutoDesk Official Training Guide “Autocad 2010 Volume 2”, April 2009.

[20] AutoDesSys “Bonzai 3d Online Manual”.

[21] http: www.antenna-theory.com.

[22] Constantine A. Balanis "Antenna Theory: Analysis and Design", 3rd Edition, 1999.

[23] Enver G. Kilinc, Catherine Dehollain, "Design and Optimization of Inductive Power Transmission for Implantable Sensor System", Symbolic and Numerical Methods, Modeling and Applications to Circuit Design (SM2ACD), 2010 XIth International Workshop on 4-6 Oct, 2010.

[24] Eui-Jung Yun, Jae-Wook Kim, Won-Gook Lee, Young-Jin Kim, Hyeong-Sik Park "Analytical estimation of high-frequency properties of RF micro-inductors prepared by direct-write techniques", Springer Science + Business Media, LLC 2007.

[25] M. Bartek, S.M. Sinaga, J.N. Burghartz "Influence of via-connections on electrical performance of vertically-spaced RF passives", Electronic Components and Technology Conference, 2005.

[26] Amal Zaki "Design and Fabrication of High-Q Spiral Inductors Using MEMS Technology", Proceedings of the 4th WSEAS Int. Conference on Electromagnetics, Wireless and Optical Communications, Venice, Italy, November 20-22, 2006.

[27] Jr-Wei Lin, C. C. Chen, and Yu-Ting Cheng, Member, IEEE "A Robust High-Q Micromachined RF Inductor for RFIC Applications", IEEE Transactions on Electron Devices, Vol. 52, No. 7, July 2005.

[28] Kenichi Okada and Kazuya Masu "Modeling of Spiral Inductors", Tokyo Institute of Technology, Japan.

[29] Steve McFee and Dennis Giannacopoulos, "Introduction to Adaptive Finite Element Analysis for Electromagnetic Simulations", Technical Article, Department of Electrical & Computer Engineering, McGill University, Canada.

[30] Anthony Nikola Laskovski, Mehmet Rasit Yuce, Tharaka Dissanayake "Stacked Spirals for Biosensor Telemetry", IEEE Sensors Journal, Vol. 11, NO. 6, June 2011.

[31] http:www.google.com

## BIOGRAPHICAL INFORMATION

Safwan Ahmed Muneer was born in Bangalore, Karnataka, India. He obtained his Bachelor's degree in Electronics and Communication Engineering in 2009, from Visweswaraiah Technological University, Belgaum, Karnataka, India. He has worked towards his Master of Science in Electrical Engineering in The University of Texas at Arlington since August 2010. His Research areas include Antenna Design and Wireless radio frequency Communication.